# LIPOSOMAL ACTINIUM-225 AS A POTENTIAL CANCER THERAPEUTIC

By

CHARLES ZHU

A dissertation submitted to the Graduate School-New Brunswick

And

The Graduate School of Biomedical Sciences

Rutgers, The State University of New Jersey

In partial fulfillment of the requirements

For the degree of

Doctor of Philosophy

Graduate Program in Biomedical Engineering

Written under the direction of

Stavroula Sofou

And approved by

_____

_____

_____

_____

New Brunswick, New Jersey

January 2017

ABSTRACT OF THE DISSERTATION

Liposomal Actinium-225 as a Potential Cancer Therapeutic

By CHARLES ZHU

Dissertation Director:

Stavroula Sofou

Alpha-particle emitting radionuclides are a promising class of emitters for the treatment of cancer. Emitted alpha-particles deposit considerable energy along a short-ranged trajectory (<100 μm), allowing the potential for highly localized and cytotoxic irradiation of cancer while sparing the surrounding healthy tissues from off-target effects. The majority of alpha-particle therapies under development are radioimmunoconjugates, which are effective in treating easily-accessible or volumetrically small target sites such as tumor vasculature, micrometastases, or liquid tumors such as leukemia. However, radiolabeled antibodies possess certain limitations such as low specific activity and potentially sub-optimal intracellular localization. Additionally, the limited penetration of solid tumor mass due to the binding site barrier effect combined with short alpha-particle trajectory effectively precludes the use of alpha-particle radioimmunoconjugates from effectively treating bulky solid tumors. To date, the use of liposome-mediated delivery of alpha-particle emitters to overcome these limitations has not been explored.

In this dissertation, we describe delivery of the alpha-particle emitting radionuclide Actinium-225 ($^{225}$Ac) mediated with liposomal nanoparticles. We investigate the anti-solid

tumor potential of $^{225}$Ac-liposomes by evaluating its efficacy against analogues of tumor vasculature and avascular solid tumors. Overall, our results suggest the feasibility of a liposomal approach in the therapy of solid, vascularized tumors.

## ACKNOWLEDGEMENTS

I would first like to thank my dissertation advisor, Dr. Stavroula Sofou, for guiding me throughout the entirety of the PhD process. She has always pushed me towards scientific excellence, and it is only through her mentorship that I was able to complete this work. I would also like to thank my committee members, Dr. Martin Yarmush, Dr. Charles Roth, and Dr. Michael McDevitt for their continual support and scientific feedback in the work that comprises this dissertation.

My colleagues, both past and present, have been instrumental in helping and supporting me throughout this process. More specifically, I would like to thank Dr. Amey Bandekar and Ana Gomez, both of whom former Sofou Lab members, for teaching me everything I needed to know to work in the lab during my first 2 years. I want to thank Michelle Sempkowski, Sarah Stras, Trevan Locke, Thomas Linz, and Alaina Howe for always being available to provide me constant support. I especially want to thank Michelle Sempkowski for helping me execute many of my project experiments and allowing me to steal her phosphate buffered saline without retaliation.

Finally, I would like to thank my family. My parents, Jianwei and Weimin Zhu supported and raised me to be the person I am today, and it would be impossible for me to overstate their role in my life. My brother, David Zhu, and I shared many good memories as children and as “adults” that act like children. He is also a reminder that I could have come into this world as a less intelligent and less handsome person (that was a joke). My wife, Audrey Wang, has supported me with her unwavering love, and at times I feel I would not been able to complete this dissertation without her.

## TABLE OF CONTENTS

## LIST OF FIGURES

**LIST OF TABLES**

# CHAPTER 1: INTRODUCTION

## 1.1: Solid, vascularized tumors

Cancer is a serious disease that caused 22.9% of all deaths in 2011 and carries a lifetime development risk of 39.6% in the United States [1]. Although cancer patient survival rates are improving with advances in technologies to detect, diagnose, and treat the disease at early stages, prognosis remains poor for patients with advanced cancer characterized by solid, vascularized tumors. In these cases, tumors access their hosts' vascular supply via angiogenesis, grow to large sizes by overcoming local diffusion limitations of oxygen and nutrients, and have high metastatic potential.

## 1.2: Current radiopharmaceutical therapy

Radiopharmaceuticals are systemically administered isotopes that release alpha- or beta-particles and deposit cytotoxic energy along their emission trajectory, and have been identified as promising drug candidates for cancer therapy. Currently, the beta-emitters Iodine-131 ($^{131}$I), Yttrium-90 ($^{90}$Y), and Lutetium-177 ($^{177}$Lu) are the predominant isotopes in therapies that have been approved or are in late-stage clinical development for a variety of indications. Orally-delivered $^{131}$I capsules are commonly used for thyroid disease and $^{131}$I-BC8 (Iomab™-B) and $^{131}$I-tositumomab (Bexxar®) are undergoing Phase III clinical trials [2] and are FDA-approved, respectively. Ibritumomab Tiuxetan delivering $^{90}$Y (Zevalin®) is FDA-approved for various types of lymphoma. Somatostatin analogues delivering $^{177}$Lu are nearing regulatory approval and show improved therapeutic efficacy with acceptable toxicities in patients with neuroendocrine tumors. Radium-223 ($^{223}$Ra) dichloride improves survival in prostate cancer patients with

bone metastases and is currently the only approved alpha-particle emitter. Other products using the alpha-emitters Astatine-211 ($^{211}$At) [3], Lead-212/Bismuth-212 ($^{212}$Pb/$^{212}$Bi) [4], Bismuth-213 ($^{213}$Bi) [5], or Actinium-225 ($^{225}$Ac) [5] have or are undergoing clinical development for various indications.

Major scientific and clinically-relevant differences between beta- and alpha-particle emissions include their cytotoxicity and tissue penetration. Beta-particles exhibit low linear energy transfer (LET; 0.1 – 1 keV/μm) along a relatively long-range trajectory (0.5 – 50 mm) resulting in low energy deposition at the disease site and the potential for off-target irradiation of large volumes of healthy tissue [6, 7]. The issue of long-range tissue penetration of beta emissions is one explanation for the shift from $^{90}$Y (average range: 39 mm) to $^{177}$Lu (average range: 0.7 mm) in clinical applications and subsequently reduced toxicity profiles. Beta-emitter therapy produces mostly easy-to-repair single-strand DNA breaks and is reliant on the creation of reactive oxygen species (ROS) to some degree to achieve tumor cell killing [8]. Therefore, tumor oxygenation state is an important factor in beta-particle therapy. However, solid tumor microenvironments frequently contain hypoxic regions in deeper, more difficult-to-treat tumor volumes, which grant those cells increased resistance to low LET radiation originating from beta-emitters or an external beam. In contrast to beta-particles, alpha-particles deposit considerably higher LET (80 – 120 keV/ μm) over a very short range (<90 μm), resulting in the potential for high levels of localized irradiation at the disease site that spares surrounding tissues from off-target effects [6, 7]. Additionally, alpha-particles are highly lethal: traversal of alpha particles through a cancer cell nucleus results in difficult-to-

repair double-strand DNA breaks and as few as 4-5 trajectories through the nucleus is sufficient for oxygen- and cell cycle-independent killing [9-11].

Alpha particle therapy however, does have potential disadvantages. The short range emissions have traditionally limited the use of alpha-emitters against disease sites small enough such that the entire area can be irradiated with a 40 – 90 μm trajectory (e.g. tumor vasculature, liquid tumors, and micrometastases). Barriers to successful drug delivery such as poor drug penetration of nanocarriers within solid tumors resulting in heterogeneous and partial tumor irradiation [12, 13] typically call for the use of longer-range beta emissions. The limited tumor penetration range is overcome by the long-range beta emission, eliminating the need for homogeneous nanocarrier distribution throughout the tumor volume [14]. However, the long-range emissions still result in significant off-target effects and toxicities, and the low LET radiation does not effectively kill hypoxic tumor regions. Given the high LET radiation, short tissue penetration of emissions, and oxygen-independent cell kill of alpha-particles, a nanocarrier that improves drug penetration of alpha-emitters has potential to effectively treat the solid tumor mass, ultimately resulting in a potential paradigm shift in how solid tumors may be treated with radiopharmaceuticals.

### 1.3: Actinium-225 ($^{225}$Ac) as a cancer therapeutic

The alpha-particle emitter $^{225}$Ac is a novel radioisotope of interest for cancer therapy. Several development programs are currently investigating $^{225}$Ac as a cancer therapeutic, the most advanced being a Phase I/II clinical trial of $^{225}$Ac-BC8 (Actimab™) [15] for acute myeloid leukemia. The isotope decays with a 10 day half-life through

Francium-221 ($^{221}$Fr; $t_{1/2}$: 4.9 min), Astatine-217 ($^{217}$At; $t_{1/2}$: 32 ms), Bismuth-213 ($^{213}$Bi; $t_{1/2}$: 45.6 min), and Bismuth-209 ($^{209}$Bi; stable), releasing a total of 4 highly energetic (99 – 120 keV/ μm) and short-range (<90 μm) alpha particles [16]. Stable association with the metal chelator 1,4,7,10-tetraazacyclododecane-1,4,7,10-tetraacetic acid (DOTA) allows the $^{225}$Ac-DOTA construct to be delivered via nanocarriers (e.g. antibodies, nanoparticles), as DOTA itself can be functionalized and covalently bound via click chemistry [17]. $^{225}$Ac-DOTA itself is rapidly excreted through the urine, reducing potential toxicities associated with metal chelates that escape the nanocarrier [18].

The use of $^{225}$Ac has several advantages. A 10 day half-life allows ample time for radiolabeling and handling of $^{225}$Ac constructs while avoiding classification as long-lived radioactive waste and logistical difficulties associated with short-lived isotopes (e.g. $^{213}$Bi, $t_{1/2}$ ~45.6 min). The release of 4 high-energy, short-range alpha particles translates to high therapeutic efficacy, particularly when compared to single alpha-particle emitting radionuclides such as $^{213}$Bi. One possible issue associated with the $^{225}$Ac decay chain during the first preclinical *in vivo* studies was the uptake of longer-lived daughter isotope $^{213}$Bi ($t_{1/2}$: 45.6 min) within the kidneys. The recoil energy of $^{225}$Ac decay results in daughter isotope escape from DOTA, and $^{213}$Bi binding to serum transferrin promotes renal uptake and high kidney dose [19-22]. Although nephrotoxicity due to $^{213}$Bi is a dose-limiting factor in preclinical animal models [23], the same problem was not observed during human use, where myelosuppression was the major toxicity [24]. Regardless, multiple strategies to retain recoiling daughters have been investigated including encapsulation of $^{225}$Ac within multivesicular liposomes [25], polymer vesicles [26], and lanthanum phosphate nanoparticles [27, 28].

### 1.4: Liposome-based delivery systems

Liposomes are lipid vesicles composed of a phospholipid bilayer encapsulating an internal aqueous space and have proven to be effective and versatile drug delivery carriers [29]. Modification of surface characteristics such as PEGylation or electrostatic charge can alter pharmacokinetics and the biodistributions to meet the specific needs of each therapy. Investigators can alter the lipid bilayer composition to have highly stable membranes that retain encapsulated drugs for weeks, or make them sensitive to external stimuli such as increased temperature or acidic pH to trigger site-specific drug release [30-35]. Functionalization of liposomes with antibodies, peptides, or small molecule ligands can improve binding onto disease sites expressing target receptors of interest such as human epidermal growth factor receptor 2 (HER2) or prostate specific membrane antigen (PSMA). In the clinical realm, several liposomal formulations of traditional chemotherapeutics such as doxorubicin, cisplatin, paclitaxel, and irinotecan exhibit improved biodistribution, pharmacokinetics, and toxicity profiles relative to their corresponding small molecule counterparts, and some have received FDA market approval [29].

To date, a liposomal construct of $^{225}$Ac has yet to be developed. Chang et al. first described a method of actively loading $^{225}$Ac into liposomes against its concentration gradient[36]. In this study, the authors combined calcium ionophore A23187 (pKa ~6.7) with the free $Ac^{3+}$ ion at pH 7.4, which allows transport of the $^{225}$Ac-A23187 resultant complex across a liposome membrane where the $^{225}$Ac is chelated to 1,4,7,10-tetraazacyclododecane-1,4,7,10-tetraacetic acid (DOTA) following dissociation of the

$^{225}$Ac-A23187 complex. This method allows for potentially 3 Actinium ions per 2 liposomes. In contrast, radiolabeled antibodies have relatively poor specific activity (1 Actinium per 800 – 2000 antibodies [17], or 1 Actinium per 25 antibodies with a newer labeling method [37]), which is a potential issue as radiolabeled antibody cell killing is dependent upon specific activity [38].

**1.5 Dissertation Summary**

The aim of this dissertation is to investigate the potential of $^{225}$Ac-loaded liposomes for therapy of solid, vascularized tumors. We hypothesize that $^{225}$Ac liposomes can be a safe and effective cancer therapy. We tested our hypothesis with the following specific aims:

1.) To determine the potential of $^{225}$Ac-loaded liposomes in treating tumor vasculature and compare efficacy to that of $^{225}$Ac-antibody constructs,
2.) To investigate the role of intracellular trafficking on the therapeutic efficacy of targeted $^{225}$Ac therapy against tumor vasculature, and
3.) To overcome the traditional limitations of alpha-particle therapy against large, solid tumors using environmentally-responsive liposomes.

In Chapter 2, we determined the potential of anti-vascular $^{225}$Ac-liposomes on human umbilical vein endothelial cells (HUVEC) induced to express PSMA and mimic tumor vasculature in an *in vitro* setting [39]. HUVEC cultured under normal conditions more closely resemble healthy vasculature. Nanocarriers (liposomes and antibodies) targeting PSMA and encapsulating $^{225}$Ac were used to treat monolayers of HUVEC (no or low PSMA expression), MatLu (moderate PSMA expression), and LNCaP (high

PSMA expression). We observed that anti-vascular $^{225}$Ac-liposomes were as effective as $^{225}$Ac-antibodies in treating tumor vasculature and left healthy vasculature relatively unharmed (>80% viability).

In Chapter 3, we investigated the role of intracellular trafficking on $^{225}$Ac therapy of tumor vasculature *in vitro*. We observed that our anti-vascular liposomes delivered less $^{225}$Ac per cell than $^{225}$Ac-antibodies, yet exhibited similar cell kill. Confocal microscopy imaging of fluorescent liposome and antibody uptake into PSMA-expressing HUVEC showed perinuclear localization of liposome constructs, which was not observed for antibodies. These data suggest that the higher cell kill per unit of liposome-delivered radioactivity may be attributed to the intracellular trafficking of liposomes, as closer nuclear proximity increases the probability of cell nucleus traversal of an ejected alpha particle and increases nucleus absorbed dose. Alpha particle traversals through a cell nucleus are very lethal: as few as 4 alpha particle trajectories across the cell nucleus at x keV/μm energy resulted in complete cell kill (reference from my review). Additionally, as many as 32 alpha particle hits at 90 keV/μm energy through the cytoplasm, although mutagenic, resulted in 70% cell viability of $A_L$ cells [40], whereas as few as 1 alpha particle through the nucleus achieved the same killing[41].

In Chapter 4, we utilized environmentally responsive liposomes without a targeting ligand to improve penetration of $^{225}$Ac-chelates and overcome the traditional limitations of alpha-particle therapy of solid tumors. Successful nanocarrier-mediated delivery of alpha particle emitters, similar to that of chemotherapeutics, is hampered by the low diffusivities of those nanocarriers through the tumor interstitium, resulting in poor drug penetration and heterogeneous tumor exposure to drug. Numerous approaches

have been investigated to overcome this challenge, including those that take advantage of the enhanced permeability and retention (EPR) effect of nanoparticles combined with a triggered release mechanism that exploits high diffusivities of small molecule therapeutics to more homogenously treat tumors [30, 34, 42, 43]. By engineering liposomes triggered to release highly diffusive $^{225}$Ac-DOTA chelates within the tumor interstitium, we were able to observe irradiation deep into the mass of large multicellular spheroids, which did not occur when $^{225}$Ac was delivered via antibodies or non-environmentally responsive liposomes. This phenomenon translated to improved tumor kill of large spheroids, even in cases of receptor overexpression and treatment with corresponding radiolabeled antibody.

# CHAPTER 2: ACTINIUM-225 LIPOSOMES FOR TARGETED ANTI-VASCULAR THERAPY

Note: data in this chapter was adapted from the following publication:

1.) Bandekar A, **Zhu C**, Jindal R, Bruchertseifer F, Morgenstern A, Sofou S, Anti-Prostate-Specific Membrane Antigen Liposomes Loaded with $^{225}$Ac for Potential Targeted Antivascular α-Particle Therapy of Cancer, Journal of Nuclear Medicine, 2014, 55(1):107-14

## 2.1 Introduction

Solid tumors require a vascular supply to overcome diffusion-limited transport of oxygen and nutrients through tissue and grow beyond 1-2 $mm^3$ in volume [44, 45]. The goal of antivascular therapy is to eliminate or reduce the tumor blood flow by targeting its neovasculature, thereby triggering tumor cell apoptosis/necrosis [46, 47]. This chapter describes a bottom-up approach in designing an anti-vascular therapy that combines: 1.) Anti-prostate specific membrane antigen (PSMA) targeting ligands, 2.) alpha-particle emitter $^{225}$Ac as the therapeutic agent, and 3.) lipid vesicles as the drug delivery carrier.

The tumor vasculature receptor prostate-specific-membrane-antigen (PSMA) is a potential drug delivery target [48]. Despite its name, PSMA is not exclusive to prostate tissue, and is expressed among tumor vascular endothelial cells of different tumor types while being absent from healthy vasculature. The attractiveness of PSMA is demonstrated through development of several anti-PSMA targeting agents including antibodies [48, 49], aptamers [50], and small molecules [51]. PSMA targeting antibodies (e.g. J591) are undergoing clinical development to evaluate their use for imaging of

tumor vasculature via single photon emission computerized tomography (SPECT) or positron emission tomography (PET) and can be covalently bound to liposomes [52]. The A10 aptamer has previously been shown to effectively target the extracellular domain of PSMA and can be functionalized onto nanoparticles via click chemistry [53]. A urea-based small molecule ligand has demonstrated specific binding to PSMA and can be covalently bound to the phospholipid headgroup for direct incorporation into a liposome via self-assembly.

Combined with rapid binding and uptake to a disease site, alpha particle emitters have the potential for localized irradiation that spares surrounding healthy tissues. Additionally, tumor vasculature is a non-bulky disease site that can be completely irradiated by short-range alpha particles. Isotopes such as $^{211}$At and $^{213}$Bi have already been used to radiolabel anti-PSMA ligands and evaluated for anti-vascular therapies [10, 11, 54]. We choose $^{225}$Ac as it releases a total of 4 cytotoxic alpha particles, and has previously been suggested as an effective anti-vascular agent when bound to an antibody targeted to vascular endothelial cadherin [55, 56].

A23187-mediated $^{225}$Ac loading into liposomes can achieve high specific radioactivity (3 Actinium atoms per 2 liposomes) [36]. In contrast, the traditional two-step $^{225}$Ac radiolabeling of antibodies results in low specific radioactivity (1 Actinium atom per 800 – 2000 antibodies), while a more recent study describes a one-step radiolabeling reaction that can label 1 Actinium atom per 25 – 100 antibodies [37]. In both cases however, the majority of antibodies do not possess $^{225}$Ac. The specific activity of radiolabeled antibodies for targeted therapy is an important factor [38] in overall efficacy as non-labeled antibodies will compete with $^{225}$Ac-labeled antibodies for a finite

pool of target receptors, particularly in cases where the tumor endothelium exhibits low to moderate levels of PSMA expression.

In this work, liposomes were loaded with $^{225}$Ac and functionalized with PSMA-targeting agents and evaluated for their potential use in anti-tumor vascular therapy. The killing efficacy and toxicity of liposomes towards *in vitro* tumor vascular or healthy endothelium models was compared to that of a $^{225}$Ac-radiolabeled J591 antibody. This particular antibody was selected as it is a PSMA-targeting agent has been evaluated for use in prostate cancer and anti-vascular applications.

## 2.2 Materials and Methods

*Liposome Preparation*

Liposomes were prepared by combining 1,2-dinonadecanoyl-sn-glycero-3-phosphocholine (DNPC), cholesterol (chol), 1,2-distearoyl-sn-glycero-3-phosphoethanolamine-N-[methoxy(polyethyleneglycol)-2000] (ammonium salt) (DSPE-PEG), and 1,2-dipalmitoyl-sn-glycero-3-phosphoethanolamine-N-(lissamine rhodamine B sulfonyl) (ammonium salt) (DPPE-rhodamine) at a 6.6:2.8:0.5:0.1 mole ratio in a round-bottom flask. The organic solvent was removed by placing the flask in a 55°C water bath under vacuum and rotation to generate a thin lipid film, which was further dried under $N_2$ gas. The film was then hydrated with 1 mL citrate buffer (160 mM citrate, pH 4.0, with 5 mg/mL p-Isothiocyanatobenzyl-1,4,7,10- tetraazacyclododecane-1,4,7,10-tetraacetic acid (DOTA), and 12 mM ascorbic acid, all in metal-free and RNAse-free water) and incubated at 55°C for 2 hours to form multilamellar vesicles. Unilamellar vesicles were formed by extruding the suspension through two stacked polycarbonate

membranes with 100 µm pores 21 times. Extra-liposomal fluid was exchanged to 20 mM HEPES/250 mM sucrose (pH 7.4) by passing the unilamellar liposomes through a Sephadex G-50 column equilibrated with the appropriate solution.

A protocol of A23187-mediated loading of $^{225}$Ac into liposomes has previously been published. Briefly, 30 µL of $^{225}$Ac dissolved in 0.03 mM HCl was added to a 50 µL suspension of 0.185 mg/mL calcium ionophore A23187 in 50:50 mixture of water and ethanol. This 80 µL of $^{225}$Ac-A23187 suspension was then added to our liposomes and heated for 1 hour at 72°C. Upon cooling liposomes to room temperature, 50 µL of 10 mM Diethylenetriamine Pentaacetic Acid (DTPA) was added to chelate un-encapsulated $^{225}$Ac, which was then removed from the liposomes via Sephadex G-50 size exclusion chromatography column equilibrated with PBS (pH 7.4) + 1 mM ethylenediaminetetraacetic acid (EDTA).

We followed a previously reported protocol to conjugate the A10 aptamer onto our liposomes [53]. Briefly, liposomes bearing 2.5% mole fraction carboxy-PEG-lipids were activated with 80 mM 1-Ethyl-3-(3-dimethylaminopropyl)-carbodiimide (EDC) and 20 mM N-hydroxysulfosuccinimide (NHS) in the presence of RNAse-free 10 mM MES (pH 5.9) with 230 mM sucrose for 20 minutes. Liposomes activated with EDC/NHS were separated from unreacted EDC/NHS by passage through a G-50 column equilibrated with 10 mM MES (pH 5.9) with 230 mM sucrose, added to 5 nmol of A10 aptamer, and incubated for 4 hours at room temperature. Un-conjugated A10 aptamer was removed by passing the mixture through a Sepharose 4B column equilibrated with PBS (pH 7.4) + 1 mM EDTA.

We followed a previously reported protocol to conjugate antibodies onto our liposomes [57]. Briefly, liposomes bearing 2.5% mole fraction PDP-PEG-DSPE were activated with 500 mM dithiothreitol (DTT) for 30 minutes at room temperature with shaking. In parallel, 0.5 µg of antibodies were activated with 20-fold molar excess of succinimidyl-4-(p-maleimidophenyl)butyrate (SMPB) for 1 hour at room temperature with shaking. Unreacted DTT was separated via passage through a Sephadex G-50 column equilibrated with PBS (pH 7.2) + 1 mM EDTA, and unreacted SMPB was separated from antibodies via passage through PD-10 column equilibrated with PBS (pH 7.2) + 1 mM EDTA. SMPB-activated antibodies were combined with DTT-activated liposomes and incubated overnight at room temperature with shaking. Un-conjugated antibodies were separated from liposomes by passing the mixture through a Sepharose 4B column equilibrated with PBS (pH 7.4) + 1 mM EDTA.

*Antibody Radiolabeling*

Radiolabeling of J591 antibodies with $^{225}$Ac was performed as previously described [17]. Briefly, $^{225}$Ac dissolved in 0.2M HCl was added to a mixture of 714 mM tetramethylammonium acetate (TMAA), 3.6 mg/mL DOTA-isothiocyanate (DOTA-NCS), and 42.9 g/L ascorbic acid (final pH 5.5 for the mixture) and heated to 60°C for 1 hour. After the first reaction, 0.45 mg of J591 antibody was added to the mixture with 25 µL of 1M carbonate buffer (pH 9.0) and 20 µL of ascorbic acid (150 g/L), and incubated at 37°C for 1 hour. The mixture was treated with 20 µL of 10 mM DTPA and passed through a 10-DG size exclusion chromatography column equilibrated with PBS to

remove unattached $^{225}$Ac-DOTA. Radiochemical purity of the final product was assessed via instant thin layer chromatography (iTLC).

*Cell Culture*

LNCaP, MatLu, MDA-MB-231, and HUVEC were cultured and maintained per recommended conditions. Induction of PSMA on HUVEC was performed as previously described [39]. First, cell-conditioned media (CCM) was generated by incubating confluent MDA-MB-231 monolayers with serum-free RPMI-1640 cell culture media for 24 hours and filtering to remove residual cells. Matrigel™ was added to 24-well plates (150 µL per well) and incubated at 37°C for 30 minutes to solidify. HUVEC were trypsinized, resuspended in CCM, seeded into Matrigel™-coated plates (50,000 cells per well), and incubated for 18 hours at 37°C to induce PSMA expression.

*Anti-Vascular Cytotoxicity*

Cell monolayers of PSMA-induced HUVEC and HUVEC were incubated with $^{225}$Ac-J591 antibodies or $^{225}$Ac-liposomes (non-targeted or functionalized with either PSMA-targeting J591 antibodies or A10 aptamers) at radioactivities ranging from $10^{-9}$ to $10^{1}$ µCi/mL ($37 \times 10^{-9}$ to $37 \times 10^{1}$ kBq/mL). After incubating with radioactivity for either 6 or 24 hours, cell monolayers were washed with PBS, incubated in their respective cell culture media for 1 doubling time, and evaluated via (3-(4,5-dimethylthiazol-2-yl)-2,5-diphenyltetrazolium bromide assay (MTT) assay.

## 2.3 Results

*Liposome and Antibody Characterization*

Characterization results of $^{225}$Ac-loaded liposomes and antibodies are summarized in Table 2.1. Loading efficiencies of $^{225}$Ac into liposomes was 58.0% ± 4.6% (PDP-liposomes for antibody conjugation, n=5) and 85.6% ± 11.7% (carboxyl-liposomes for aptamer conjugation, n=5). Loading efficiency of $^{225}$Ac onto J591 antibodies was 2.8 ± 0.2% (n=3). Liposomes and antibodies stably retained 69.4 ± 1.2% and 86.7 ± 3.7% of initial nanocarrier-associated $^{225}$Ac after 24 hours incubation in 10% serum-supplemented media. Anti-PSMA ligand conjugation reactions resulted in either 17 ± 2 J591 antibodies per liposome (n=5), or 9 ± 2 A10 aptamers per liposome (n=5). The immunoreactivity of J591-liposomes, A10-liposomes, and J591 antibodies were determined to be 21.3 ± 3.0% (n=5), 11.2 ± 1.0% (n=5), and 76.9 ± 2.7% (n=3), respectively.

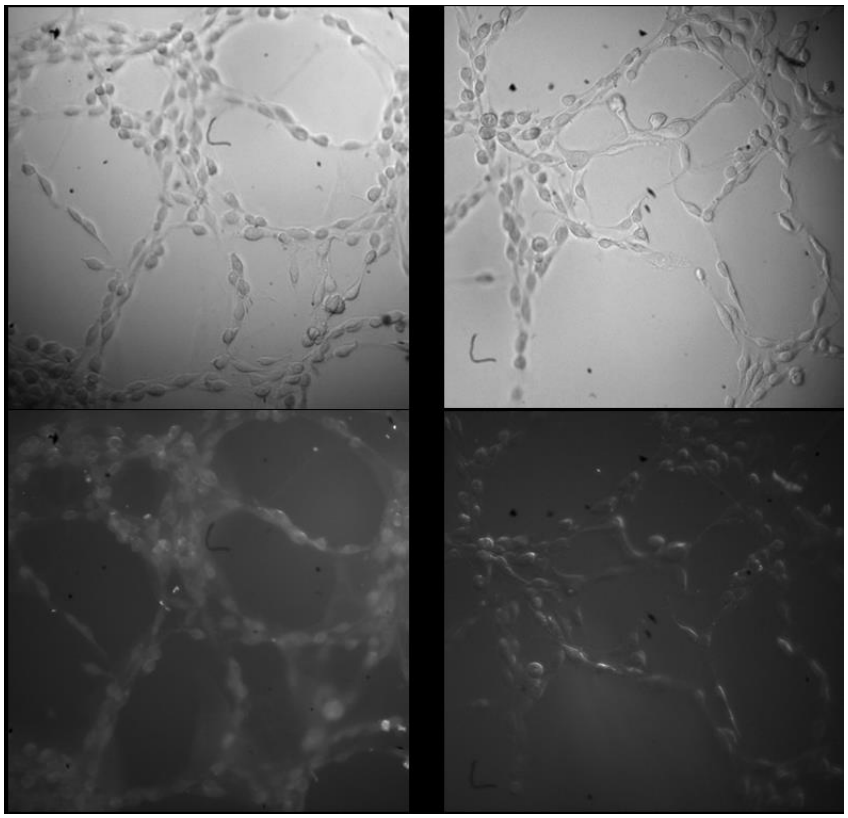

**Figure 2.1:** HUVEC monolayers cultured on Matrigel™ and in the presence of CCM (left) probed with J591 antibodies and then stained with fluorescein-labeled goat anti-mouse second antibodies under fluorescent microscopy (bottom left). HUVEC monolayers cultured on Matrigel™ in the presence of regular F-12K media did not show staining when probed with J591 and stained with the same secondary antibody (bottom right). Top panels are bright field images.

*Expression of PSMA on HUVEC*

Fluorescence microscopy showed that J591 antibodies exhibited enhanced targeting and uptake on HUVEC cultured on Matrigel™ and in the presence of CCM over HUVEC culture without CCM (Figure 2.1). These results suggest the presence of PSMA on induced HUVEC in accordance with Liu et al., who first described this system.

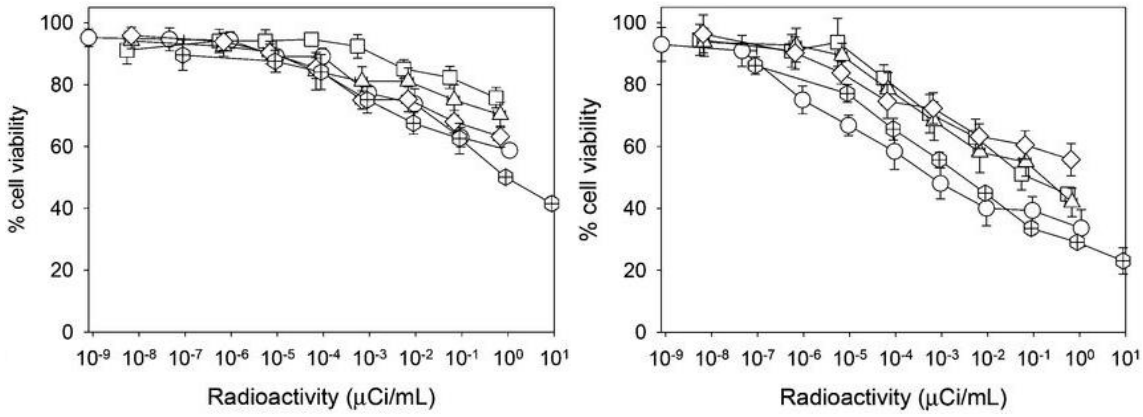


**Figure 2.2:** Efficacy of $^{225}$Ac constructs on PSMA-expressing HUVEC monolayers after 6 (left panel) or 24 (right panel) hours of incubation. The constructs of $^{225}$Ac were J591-antibody-liposomes (circles), A10-aptamer-liposomes (squares), nontargeted liposomes (triangles), small molecule $^{225}$Ac-DOTA chelate (diamonds), and $^{225}$Ac-radiolabeled J591 antibodies (crossed hexagons). Errors bars correspond to standard deviation of 2 preparations, 2 wells per preparation.

*Cytotoxicity of $^{225}$Ac-liposomes and $^{225}$Ac-J591*

The MTT viability of PSMA-expressing HUVEC and HUVEC under normal culture conditions after exposure to a variety of $^{225}$Ac constructs are shown in Figures 2.2 and 2.3. After 6 hours of incubation on PSMA-expressing HUVEC monolayers, radiolabeled J591 antibodies exhibited the most cytotoxicity of the studied constructs with an observed $LD_{50}$ of 8.9 x $10^{-1}$ μCi/mL (3.3 x $10^4$ Bq/mL); the $LD_{50}$ after 6 hours incubation for all studied $^{225}$Ac-liposomes (non-targeted or functionalized with either A10-aptamer or J591 antibody) was not reached at the highest dose of radioactivity. However, at 24 hours of incubation, J591-liposomes exhibited similar cytotoxicity with a $LD_{50}$ of 6.3 x $10^{-4}$ μCi/mL (2.3 x $10^1$ Bq/mL) when compared to radiolabeled J591 antibodies ($LD_{50}$: 3.0 x $10^{-3}$ μCi/mL or 1.1 x $10^2$ Bq/mL, $P > 0.05$), and greater cytotoxicity than that of A10-liposomes ($LD_{50}$: 1.1 x $10^{-1}$ μCi/mL or 4.1 x $10^3$ Bq/mL, P<

0.05), and non-targeted liposomes ($LD_{50}$: 1.5 x $10^{-1}$ μCi/mL or 5.6 x $10^{3}$ Bq/mL, P < 0.05).

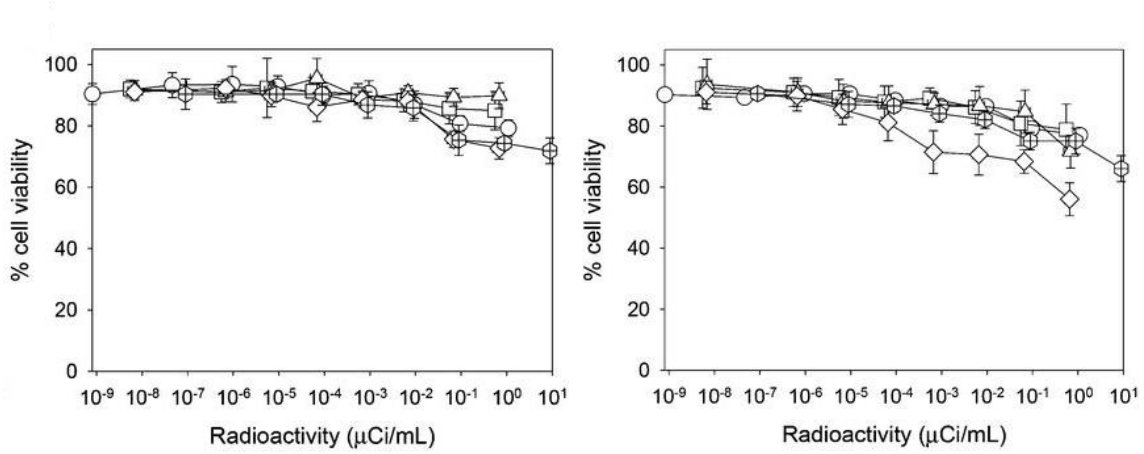


**Figure 2.3:** Toxicity of $^{225}$Ac constructs on PSMA-negative HUVEC monolayers after 6 (left panel) or 24 (right panel) hours of incubation. The constructs of $^{225}$Ac were J591-antibody-liposomes (circles), A10-aptamer-liposomes (squares), nontargeted liposomes (triangles), small molecule $^{225}$Ac-DOTA chelate (diamonds), and $^{225}$Ac-radiolabeled J591 antibodies (crossed hexagons). Errors bars correspond to standard deviation of 2 preparations, 2 wells per preparation.

On HUVEC cultured under normal conditions and in the absence of Matrigel™, the $LD_{50}$ was not reached for any of the studied constructs at either 6 or 24 hours. (Figure 2.3).

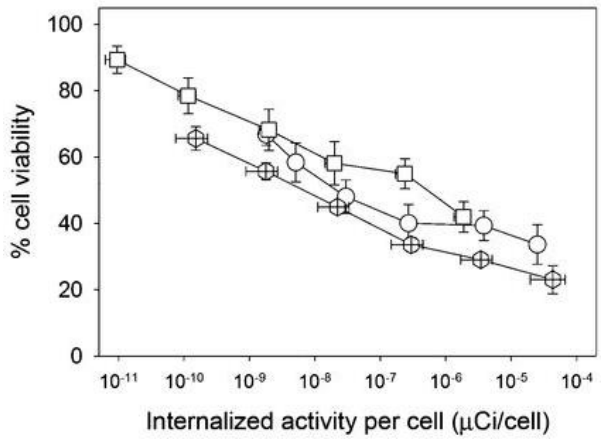


**Figure 2.4:** Cell viability as a function of cell internalized radioactivity delivered via J591-antibody-liposomes (circles), A10-aptamer-liposomes (squares), and J591 antibodies (crossed hexagons) after 24 hours of incubation on PSMA-expressing HUVEC. Errors bars correspond to standard deviation of 2 preparations, 2 wells per preparation.

The cell viability of PSMA-expressing HUVEC as a function of internalized $^{225}$Ac delivered via J591 antibodies, J591-antibody-liposomes, or A10-aptamer-liposomes is shown in Figure 2.4. Our results showed that $^{225}$Ac delivered via J591 antibodies exhibited the greatest efficacy per unit of delivered radioactivity, followed by the targeted liposomal constructs.

## 2.4 Discussion

In this chapter, we evaluated the potential of $^{225}$Ac-loaded, PSMA-targeted liposomes to selectively kill PSMA-expressing HUVEC monolayers. We investigated two distinct targeting ligands (antibodies and aptamers) on liposomes and demonstrated the superiority of J591-antibody-liposomes over A10-aptamer-liposomes and non-

targeted liposomes with respect to their reactivity towards PSMA and cytotoxicity/$LD_{50}$ dose towards PSMA-expressing endothelial cells *in vitro*.

One interesting phenomenon we observed was the differences in cell viability as a function of cell-internalized radioactivity between different constructs. The differences in efficacy per delivered radioactivity could be potentially attributed to differences in intracellular trafficking and cellular localization. Given that each alpha-particle is ejected in a random direction in 3D space upon isotope decay and the short range of each alpha particle trajectory, the location of such an event within a cell would influence the probability of an emission crossing the nucleus and therefore affect killing efficacy. We explore this phenomenon in greater detail in the next chapter.

# CHAPTER 3: INTRACELLULAR LOCALIZATION OF ACTINIUM-225 AFFECTS EFFICACY

Note: data in this chapter was adapted from the following publications:

2.) **Zhu C**, Bandekar A, Sempkowski M, Banerjee SR, Pomper MG, Bruchertseifer F, Morgenstern A, Sofou S, Nanoconjugation of PSMA-Targeting Ligands Enhances Perinuclear Localization and Improves Efficacy of Delivered Alpha-Particle Emitters against Tumor Endothelial Analogues, Molecular Cancer Therapeutics, 2016, 15(1):106-13

3.) Bandekar A, **Zhu C**, Jindal R, Bruchertseifer F, Morgenstern A, Sofou S, Anti-Prostate-Specific Membrane Antigen Liposomes Loaded with $^{225}$Ac for Potential Targeted Antivascular α-Particle Therapy of Cancer, Journal of Nuclear Medicine, 2014, 55(1):107-14

## 3.1 Introduction

Alpha particle emitters such as $^{225}$Ac are recognized to be highly lethal drugs that deliver their dose in a localized fashion and have potential to be effective therapeutics for antivascular applications in cancer treatment [7, 20, 52, 58]. Work described in the previous chapter of this dissertation as well as in Bandekar et al. 2014 [52] established the anti-vascular potential of $^{225}$Ac-loaded liposomes targeted to Prostate Specific Membrane Antigen (PSMA). The optimization of intracellular distribution/trafficking of alpha-particle emitters may further improve their killing efficacy against targets like tumor vasculature.

Intracellular distribution and trafficking of radionuclides are critical considerations for certain emissions such as Auger electrons [59], which possess an extremely short tissue range (on the order of nanometers); localization far from a cell nucleus would result in no direct DNA damage. Given the longer range of alpha-particles (<100 μm), intracellular distribution is not as critical of a concern and has traditionally been overlooked. However, radionuclides still eject alpha-particles in a random direction through 3D space, and DNA-damaging alpha-particles do most cellular damage when crossing the nucleus as opposed to other spaces within the cytoplasm [40, 41]. Therefore, the intracellular distribution of $^{225}$Ac after specific uptake will affect the probability of a nuclear hit of an emitted alpha particle and the corresponding cell viability.

We hypothesize that altering the intracellular distribution of targeted antivascular nanocarriers to enhance perinuclear localization will result in similarly enhanced efficacy of delivered $^{225}$Ac. We test our hypothesis using liposomes loaded with $^{225}$Ac and functionalized with PSMA-targeting ligands (fully human mAb targeting PSMA, and a urea-based small molecule ligand) as well as $^{225}$Ac-radiolabeled antibodies. Similar to the studies described in Chapter 2, Human Umbilical Vein Endothelial Cells (HUVEC) under either normal conditions or triggered to express PSMA constituted our *in vitro* analogue for healthy and tumor neovasculature, respectively. Preclinical studies evaluating neovasculature-targeting therapies are challenging, as human tumor endothelial cells that express human target antigens are unavailable for cell culture [60], and the neovasculature in animal tumors are host-origin. Therefore, we emulated tumor endothelium using *in vitro* analogues consisting of PSMA-expressing HUVEC monolayers under a controlled flow field. We evaluate $^{225}$Ac constructs (PSMA antibody-

and urea-ligand liposomes and radiolabeled PSMA antibodies) for PSMA targeting selectivity, killing efficacy of tumor vasculature, intracellular distribution/trafficking, and resulting double-strand DNA breaks.

## 3.2 Materials and Methods

*Synthesis of Lysine-Glutamate Urea*

Synthesis of the urea-based small molecule targeting ligand bound to a PEGylated lipid was performed by Sangeeta Ray Banerjee and Martin Pomper. A solution of N-hydroxysuccinimide ester of suberate lysine-glutamate urea (5 mg, 8.98 μmol, in 500 μL DMF) was added to 1,2-distearoyl-sn-glycero-3-phosphoethanolamine-N-[Methoxy(Polyethylene glycol)-2000] (Ammonium Salt; DSPE-PEG2000) (10 mg, 3.6 μmol in 900 μL DMF) followed by N,N-diisopropylethylamine (DIEA; 3 μL, 18 μmol). The reaction mixture was stirred at room temperature for 2 hours, and was then concentrated under reduced pressure at approximately 40°C. The semi-solid residue thus obtained was washed with 5 × 1 mL 80/20 water/acetonitrile solution to remove unreacted lysine-glutamate urea. The colorless product was dried under high vacuum for 20 hours and was used for experiments. The synthesis yield was approximately 90% and with m/Z: 1594.5 [M+1]2+ by ElectroSpray Mass Spectrometry. The molecular structure of the functionalized lipid with a non-active analogue (negative control) of the urea ligand is shown in Figure 3.1. The targeting urea molecule is a small molecule. Therefore, for the design of the negative control, a linker was attached to the lipid.

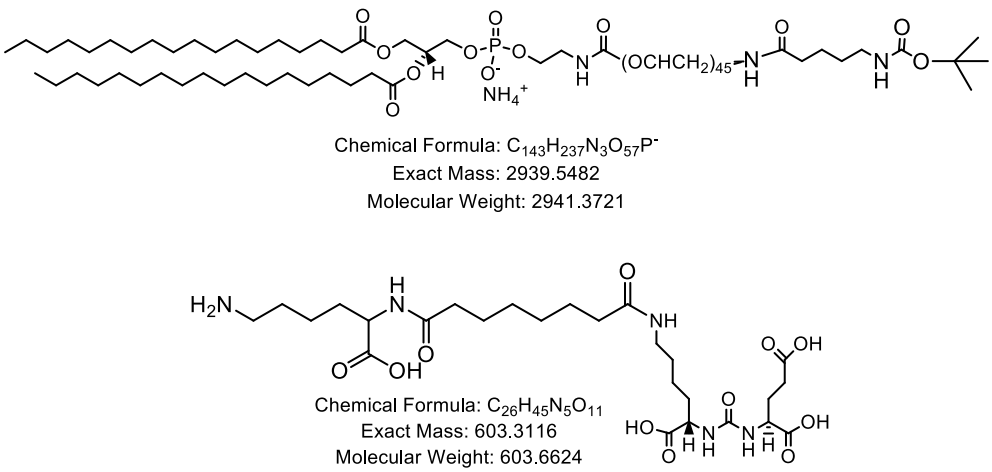


**Figure 3.1:** Chemical structure of the inactive linker (top), and the PSMA-targeting urea (bottom)

*Liposome Preparation*

The following lipids were used for liposome preparation: 2-dihenarachidoyl-sn-glycero-3-phosphocholine (21PC), 1,2-distearoyl-sn-glycero-3-phosphoethanolamine-N-[Methoxy(Polyethylene glycol)-2000] (Ammonium Salt; DSPE-PEG2000), 1,2-distearoyl-sn-glycero-3-phosphoethanolamine-N-[PDP (Polyethylene Glycol) 2000] (Ammonium Salt; DSPE-PEG-PDP), 1,2-dipalmitoyl-sn-glycero-3-phosphoethanolamine-N-(LissamineRhodamine B Sulfonyl) (Ammonium Salt; DPPE-Rhodamine), and cholesterol (chol).

Nontargeted liposomes were composed of a 66.0:28.3:4.7:1.0 mole ratio of 21PC:chol:DSPE-PEG2000:DPPE-Rhodamine. For antibody-targeted liposomes, 1 mole % of DSPE-PEG2000 was replaced with DSPE-PEG-PDP. For urea-targeted liposomes, 0.5 mole % of the lysine-glutamate urea-based lipid was included on the liposomes. All components were dissolved in chloroform or a chloroform-methanol mixture and combined in a round bottom flask. Lipid mixtures were dried under vacuum and rotation

at 55°C followed by further drying under $N_2$ gas to yield a thin film. Lipids were hydrated in citrate buffer (140 mM citrate, 5 mg/mL DOTA, 2.1 mg/mL ascorbic acid, pH 5.0) and incubated at 55°C for 2 hours. The suspension was extruded 21 times through two polycarbonate membranes with 100 nm pore diameter, and eluted through a Sepharose 4B column with HEPES buffer (20 mM HEPES, 250 mM sucrose, pH 7.4). Liposome size and polydispersity index were determined using a Zetasizer NanoSeries.

Loading of $^{225}$Ac into liposomes was accomplished similarly as previously described [36, 52]. Briefly, 80 µL of a mixture containing 30 µL of $^{225}$Ac dissolved in 0.03 mM HCl and 50 µL of 0.37 mg/mL calcium ionophore A23187 in a 1:1 mixture of metal-free water and ethanol to 1 mL of liposomes (5 mM total lipid). After incubating the liposome-$^{225}$Ac-A23187 mixture for 1 hour at 80 °C, 50 µL of DTPA was added to chelate unentrapped $^{225}$Ac, and the entire volume was passed through a Sephadex G50 column eluted with phosphate buffered saline (PBS) + 1 mM Ethylenediaminetetraacetic acid (EDTA) to separate liposomes from un-encapsulated $^{225}$Ac.

*Antibody Radiolabeling*

Antibody radiolabeling was performed as previously described in literature [17] and in Chapter 2 of this dissertation. Briefly, $^{225}$Ac dissolved in 0.2 M HCl was added to a mixture of 714 mM tetramethylammonium acetate (TMAA), 3.6 mg/mL DOTA-isothiocyanate (DOTA-NCS), and 42.9 g/L ascorbic acid (final pH 5.5 for the mixture) and heated to 60°C for 1 hour. Antibodies (0.45 mg) was added to the mixture with 25 µL of 1M carbonate buffer (pH 9.0), 20 µL of ascorbic acid (150 g/L), and incubated at 37°C for 1 hour. The mixture was treated with 20 µL of 10 mM DTPA and passed through a

10-DG size exclusion chromatography column equilibrated with PBS + 1 mM EDTA to remove unconjugated $^{225}$Ac-DOTA. Radiochemical purity of the final product was assessed via instant thin layer chromatography (iTLC) using 10 mM EDTA as the mobile phase.

Antibodies were radiolabeled with Indium-111 ($^{111}$In) for receptor counting experiments. Briefly, isothiocyanate-functionalized DTPA was added to anti-PSMA antibodies at a 15:1 mole ratio in 1 M carbonate buffer (pH 9.0) and incubated overnight with shaking. Antibody-DTPA conjugates were separated from unreacted DTPA by eluting the mixture through a 10-DG column with 1 M acetate buffer (pH 4.5). $^{111}$In dissolved in 0.2 M HCl was added to the mixture, which was heated to 37°C for 1 hour. Free $^{111}$In was removed from radiolabeled antibodies by first adding 50 µL of 10 mM EDTA to the mixture, then eluting it through a 10-DG column with PBS + 1 mM EDTA. Radiochemical purity of the final product was assessed via instant thin layer chromatography (iTLC) using 10 mM EDTA as the mobile phase.

*Characterization of Targeted Constructs*

The immunoreactive fraction of PSMA-targeting liposomes (antibody- and urea-ligand) and PSMA-targeting antibodies was determined by incubating the appropriate construct in a 100-fold molar excess of PSMA receptors on LnCaP cells. The apparent binding affinity/dissociation constant $K_D$ was evaluated on 4% paraformaldehyde-fixed, PSMA-expressing HUVEC by measuring cell-associated radioactivity using serial dilutions of $^{225}$Ac-loaded constructs.

*Induction of PSMA Expression on HUVEC*

Induction of PSMA on HUVEC was performed as previously described in literature [39] and in Chapter 2 of this dissertation. First, cell-conditioned media (CCM) was generated by incubating confluent MDA-MB-231 monolayers with serum-free RPMI-1640 cell culture media for 24 hours and filtering to remove residual cells. Matrigel™ was added to a rectangular chamber (for either static or parallel plate flow experiments) and allowed to solidify for 30 minutes. HUVEC were trypsinized, resuspended in CCM, and allowed to incubate on solidified Matrigel™ for 18 hours at 37°C to induce PSMA expression.

The successful induction of PSMA was determined with immunofluorescence staining followed by detection via flow cytometry, and Western Blot. For flow cytometry analysis, HUVEC were fixed with 4% paraformaldehyde, separated from Matrigel ™ via centrifugation, and incubated for 60 minutes with a mouse anti-human PSMA antibody followed by 60 minutes with a fluorescein-labeled goat anti-mouse secondary antibody. LnCaP (PSMA positive) and HUVEC cultured under normal conditions (PSMA negative) were similarly evaluated. For Western Blot analysis, cell lysate proteins were evaluated via SDS-PAGE under reducing conditions and transferred onto a nitrocellulose membrane. After blocking for 1 hour at room temperature with 5% non-fat dry milk in Tris buffer (20 mM Tris, 150 mM NaCl, 0.05% Tween20), the nitrocellulose membrane was probed with mouse anti-PSMA antibody, followed by a secondary goat anti-mouse IgG-horseradish peroxidase conjugate. Color was developed by adding horseradish peroxidase substrate.

*Cell-Associated Radioactivity and Viability*

Association of $^{225}$Ac constructs to cells were evaluated either under static or flow conditions. $^{225}$Ac constructs were diluted in the appropriate cell culture media (CCM for PSMA-induced HUVEC, 10% serum-supplemented F-12K for non-PSMA-expressing HUVEC) and placed on HUVEC monolayers under either static conditions or at a constant flow rate of 0.1 mL/minute (15 $s^{-1}$ shear rate) through the parallel plate flow chamber. After a predetermined incubation time, cells were washed twice with ice-cold PBS and suspended in 10% serum-supplemented F-12K medium. Cell-associated radioactivity was measured by counting the gamma emissions of Bismuth-213 upon secular equilibrium. Viability was determined via MTT assay initiated 1 or 3 doubling times after incubation with radioactivity.

*Intracellular Localization of $^{225}$Ac Constructs*

PSMA-expressing HUVECs were incubated under static conditions with fluorescently-labeled liposomes or antibodies in the presence or absence of 10 μg/mL chlorpromazine or 100 μg/mL genistein (inhibitors of clathrin- and caveolae-mediated endocytosis, respectively). After incubation, cells were fixed with 4% paraformaldehyde, stained with nuclear dye Hoechst 33342, and washed thrice with PBS. Cells were then imaged under high resolution confocal microscopy under a 100x oil immersion objective on a Leica TCS SP2.

To quantitatively determine the intracellular distribution of nanocarrier constructs with respect to the nucleus, a dilation protocol was applied. The fluorescence of the Hoechst-stained cell nucleus was thresholded to define the nuclear boundary in each

image. A circular morphologic structuring element was used to follow the edges of the nucleus to trace concentric ring-like regions that expanded radially from the nuclear boundary. The sum of pixel intensities corresponding to fluorescent liposomes or antibodies within each ring was normalized over the total pixel intensity per cell and plotted as a function of distance from the edge of the nucleus.

*Characterization of Cellular Uptake Mechanism*

PSMA-expressing HUVEC were pre-incubated with 10 μg/mL chlorpromazine, 100 μg/mL genistein, or under CCM without endocytosis inhibitors for 30 minutes prior to exposure to fluorescently labeled liposomes or antibodies for 2 hours. After incubation, cells were washed twice with PBS, centrifuged to remove Matrigel™, and evaluated for cell-associated fluorescence using flow cytometry.

*Immunofluorescent staining of γ-H2AX foci*

After a 6-hour incubation of radioactive constructs, PSMA-expressing HUVEC were washed with PBS and fixed with 4% paraformaldehyde for 10 minutes at room temperature. Cells were then permeabilized for 5 minutes at room temperature with 0.1% Triton X-100 in PBS and stained for γ-H2AX using the OxiSelect DNA Double Strand Break kit from CellBioLabs per kit instructions.

## 3.3 Results

*Liposome Characterization*

The average liposome size was 107 ± 5 nm with a polydispersity index of 0.06 ± 0.04 (n = 12). Anti-PSMA antibody conjugation resulted in 31 ± 9 antibodies per liposome (n = 4). Optimization studies on urea-targeting liposomes were performed by Amey Bandekar indicated that approximately 368 urea ligands per liposome exhibit the best uptake. The measured immunoreactivities of $^{225}$Ac-radiolabeled antibodies, antibody-liposomes, and urea-liposomes were 88.6 ± 0.8% (n = 3), 18.1 ± 1.5% (n = 3), and 15.8 ± 1.6% (n = 3), respectively. Pre-saturation/blocking of PSMA with unlabeled antibodies resulted in limited association of antibody-liposomes (0.1 ± 0.0%) and urea-liposomes (3.9 ± 3.7%).

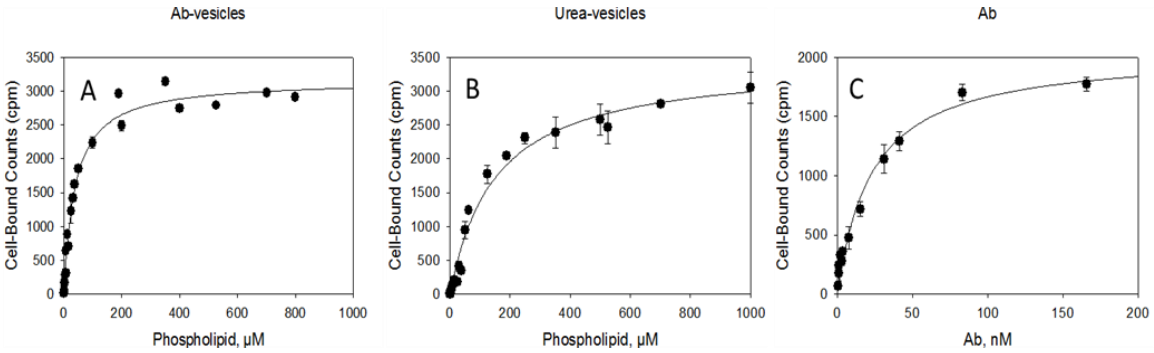


**Figure 3.2:** Dissociation constant $K_D$ of PSMA-targeting antibody-liposomes (A), urea-liposomes (B), and antibody (C). Data points represent the mean and standard deviation of repeated measurements (2 and 3 preparations for antibodies and liposomes, respectively, 2 measurements per preparation)

The equilibrium binding affinity $K_D$ was estimated using nonlinear regression for the antibody-liposomes (35.6 ± 1.5 μM), urea-liposomes (147 ± 9 μM), and $^{225}$Ac radiolabeled antibodies (22.9 ± 2.1 nM) and shown in Figure 3.2. Using $^{111}$In-labeled

PSMA antibodies, we were able to estimate the PSMA expression of induced HUVEC to be 5.2 x $10^4$ receptors per cell.

The average loading efficiency of $^{225}$Ac was 47.1 ± 16.6% for all liposome constructs (n = 16) and 3.4 ± 0.3% for antibodies (n = 2). In the presence of cells, liposomes retained 78.5 ± 3.6% of initial $^{225}$Ac (n = 16) and antibodies retained 86.3 ± 2.3% (n = 2) for the length of studies.

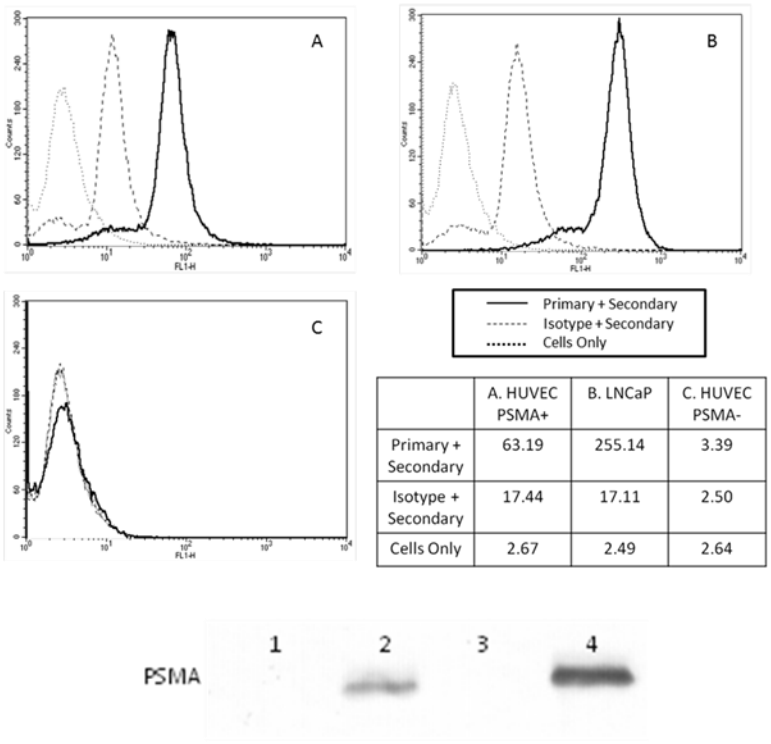


| | A. HUVEC PSMA+ | B. LNCaP | C. HUVEC PSMA- |
|---|---|---|---|
| Primary + Secondary | 63.19 | 255.14 | 3.39 |
| Isotype + Secondary | 17.44 | 17.11 | 2.50 |
| Cells Only | 2.67 | 2.49 | 2.64 |

**Figure 3.4:** PSMA expression as determined by flow cytometry (top) and Western blot (bottom). Flow cytometry panels are as follows: (A) PSMA-expressing HUVEC, (B) LnCaP, and (C) HUVEC. Western blot lanes contain: (1) HUVEC, (2) PSMA-expressing HUVEC, (3) Blank well, (4) LnCaP

*PSMA Expression by HUVEC*

Induced HUVEC seeded on Matrigel™ and in the presence of CCM exhibited a mean shift on flow cytometry of 63 compared to a shift of 3 for normal HUVEC, and exhibited positive staining by anti-PSMA antibodies on Western blot (Figure 3.4).

*Killing Efficacy and Specific Cell Association of Radioactivity*

Specific cell association of delivered radioactivity significantly increased with incubation time for all targeted constructs ($P < 0.01$). All targeted constructs delivered more activity to HUVECs under static than under flow conditions at a given time point. Both antibody- and urea-targeted liposomes delivered comparable levels of radioactivity (both cell-associated and internalized). Radiolabeled antibodies delivered significantly more $^{225}$Ac per cell than either targeted liposome construct at 4 and 6 hours incubation ($P < 0.01$; Table 3.1).

The MTT viability of PSMA-expressing HUVEC decreased with increasing exposure time to targeted $^{225}$Ac constructs (Figures 3.5A, 3.5B). This cell kill was not observed with non-targeted constructs on PSMA-expressing cells or free $^{225}$Ac-DOTA (Figures 3.5C, 3.5D), or targeted constructs on normal HUVEC that do not express PSMA (Figures 3.5E, 3.5F).

When evaluating the MTT viability of PSMA-expressing HUVEC as a function of cell-associated $^{225}$Ac, our results showed that $^{225}$Ac delivered by either of the liposomal constructs was more lethal than that delivered by antibodies per unit radioactivity (Figure 3.6)

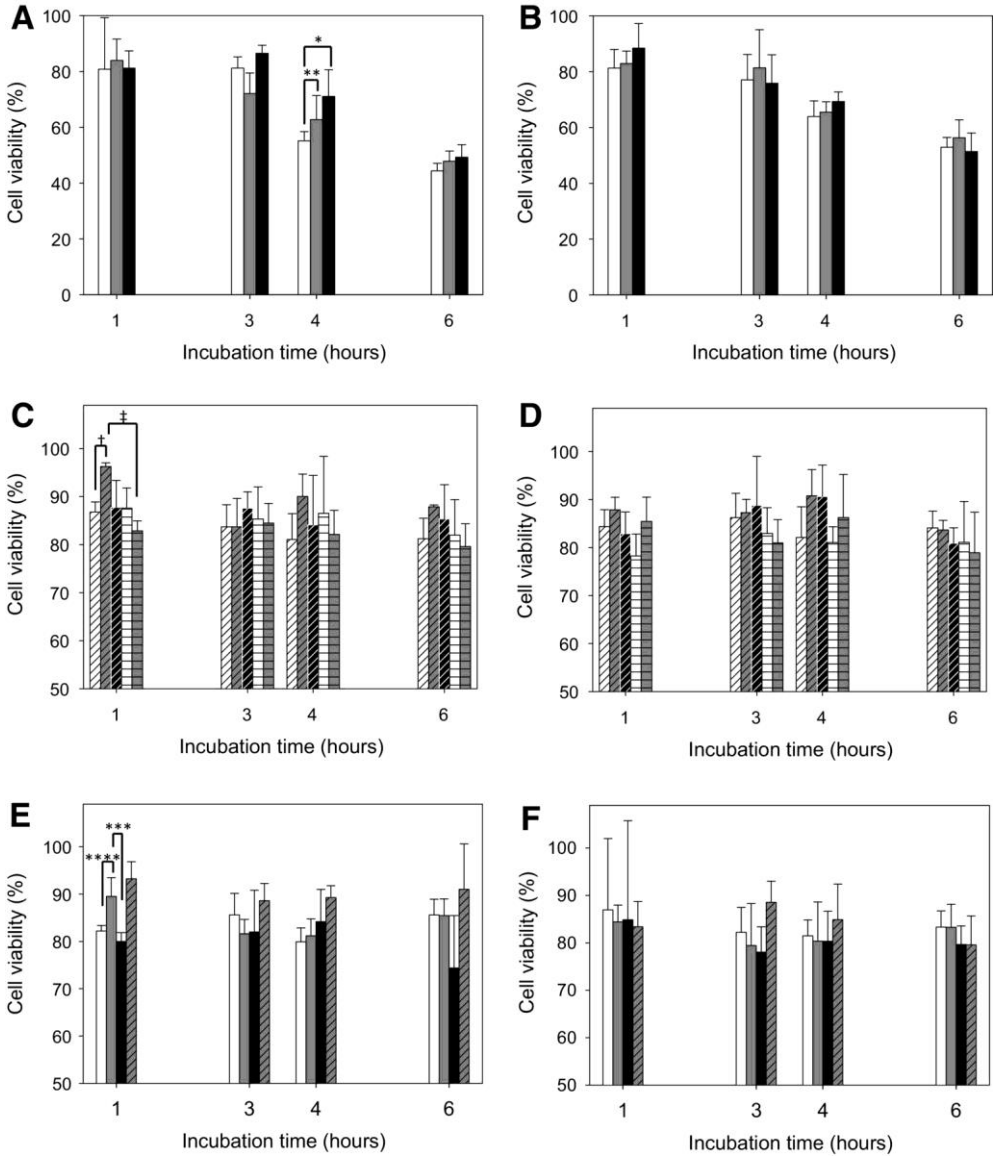


**Figure 3.5:** Viability of PSMA-positive (A–D) and PSMA-negative HUVEC (E and F) after treatment by $^{225}$Ac constructs for different incubation times in static incubation conditions (A, C, and E), and in the presence of a flow field (15 s−1 shear rate; B, D, and F). White bars, antibody-liposomes; gray bars, urea-liposomes; black bars, radiolabeled Ab; white bars with tilted pattern, non-targeted $^{225}$Ac liposomes; gray bars with tilted pattern, $^{225}$Ac-DOTA chelate at activity levels corresponding to the values released from lipid vesicles; black bars with tilted pattern, nonradiolabeled antibody. White bars with horizontal pattern, $^{225}$Ac-loaded vesicles labeled with an non-specific antibody; gray bars with horizontal pattern, $^{225}$Ac-loaded vesicles labeled with an non-active urea analog. Viability evaluated after three doubling times. Error bars, SD of repeated measurements (2 and 3 independent preparations for antibodies and for vesicles, respectively, 2 measurements per preparation; *, P = 0.044; **, P = 0.063; †, P = 0.039; ‡, P = 0.031; ***, P = 0.012; ****, P = 0.007; all other cases P > 0.12).

**Table 3.1:** Specific cell associated radioactivity ($x10^{-3}$ Bq/cell) delivered to PSMA+ HUVEC using different delivery constructs. Specific cell association is defined as the measured cell associated activities mediated by the targeted constructs corrected for non-specific cell association by subtraction of the radioactivities delivered with non-targeted vesicles. For the radiolabeled antibody, non-specific cell association is measured by the radioactivities delivered to $PSMA^-$ HUVEC cells by the same radiolabeled antibody (or by the use of a radolabeled isotype control Ab on $PSMA^+$ HUVEC)

| | | STATIC | | FLOW | |
|---|---|---|---|---|---|
| | Time of Incubation (hours) | Specifically cell associated radioactivity ; surface bound and internalized (% of total introduced radioactivity) | Specifically Internalized Radioactivity (% internalized relative to cell associated radioactivity) | Specifically cell associated radioactivity; surface bound and internalized (% of total introduced radioactivity) | Specifically Internalized Radioactivity (% internalized relative to cell associated radioactivity) |
| Antibody-labeled vesicles | 1 | 0.72±0.13 (1.9±0.4) | 0.21±0.01 (29.8±1.8) | 0.47±0.29 (1.3±0.8) | 0.07±0.07 (13.9±13.4) |
| | 3 | 1.02±0.06 (2.8±0.2) | 0.41±0.09 (39.9 ±8.8) | 0.53±0.01 (1.4±0.0) | 0.17±0.05 (31.9±10.0) |
| | 4 | 3.17±0.74 (8.6±2.0) | 2.05±0.36 (64.7±11.3) | 1.72±0.31 (4.7±0.8) | 0.97±0.19 (56.2±11.3) |
| | 6 | 4.16±0.49 (11.2±1.3) | 2.86±0.24 (68.6±5.7) | 2.10±0.45 (5.7±1.2) | 1.30±0.21 (61.7±9.8) |
| Urea-vesicles | 1 | 0.79±0.25 (2.1±0.7) | 0.08±0.02 (9.9±2.8) | 0.53±0.15 (1.4±0.4) | 0.17±0.24 (31.2±44.9) |
| | 3 | 1.03±0.44 (2.8±1.2) | 0.42±0.58 (40.4±56.2) | 0.51±0.10 (1.4±0.3) | 0.12±0.12 (24.0±23.9) |
| | 4 | 2.03±0.92 (5.5±2.5) | 1.06±0.22 (52.2±11.0) | 1.26±0.51 (3.4±1.4) | 0.47±0.03 (37.5±2.5) |
| | 6 | 3.72±0.33 (10.1±0.9) | 2.24±0.21 (60.1±5.6) | 1.91±0.41 (5.2±1.1) | 0.98±0.28 (51.4±14.7) |
| Radiolabeled Antibody | 1 | 0.96±0.61 (2.6±1.7) | 0.41±0.14 (42.6±14.3) | 0.55±0.23 (1.5±0.6) | 0.14±0.01 (25.7±1.1) |
| | 3 | 0.90±0.10 (2.4±0.3) | 0.31±0.31 (34.6±34.6) | 0.65±0.28 (1.8±0.8) | 0.40±0.05 (61.9±8.4) |
| | 4 | 10.59±0.34 (28.6±0.9) | 1.24±6.92 (50.0±11.7) | 6.92±2.58 (18.7±7.0) | 1.87±0.02 (27.1±0.3) |
| | 6 | 14.08±0.24 (38.1±0.7) | 9.77±2.68 (69.4±19.1) | 8.32±0.30 (22.5±0.8) | 3.77±0.51 (45.3±6.1) |
| | 10 | 16.77±1.62 (45.3±4.4) | 11.96±2.59 (71.3±15.5) | 9.07±0.58 (24.5±1.6) | 4.08±0.84 (44.9±9.2) |
| Antibody-vesicles on PSMA-HUVEC | 1 | 0.06±0.04 (0.2±0.1) | 0.04±0.05 (61.8±82.9) | 0.08±0.12 (0.1±0.3) | 0.03±0.05 (40.0±56.6) |
| | 6 | 0.06±0.01 (0.2±0.0) | 0.03±0.02 (57.2±39.8) | 0.09±0.03 (0.0±0.0) | 0.02±0.01 (27.3±12.9) |
| Urea-vesicles on PSMA-HUVEC | 1 | 0.05±0.01 (0.1±0.0) | 0.02±0.01 (40.4±18.1) | 0.04±0.01 (0.0±0.0) | 0.11±0.05 (280±118) |
| | 6 | 0.05±0.02 (0.1±0.1) | 0.04±0.03 (74.5±58.2) | 0.14±0.03 (0.0±0.0) | 0.06±0.03 (41.2±24.4) |
| Non-targeted vesicles on PSMA+ HUVEC | 1 | 0.12±0.02 (0.3±0.1) | 0.01±0.00 (4.2±3.2) | 0.04±0.04 (0.1±0.1) | 0.05±0.06 (129.4±159.4) |
| | 6 | 0.06±0.02 (0.2±0.1) | 0.02±0.01 (27.7±10.3) | 0.03±0.01 (0.1±0.0) | 0.01±0.01 (35.1±23.9) |

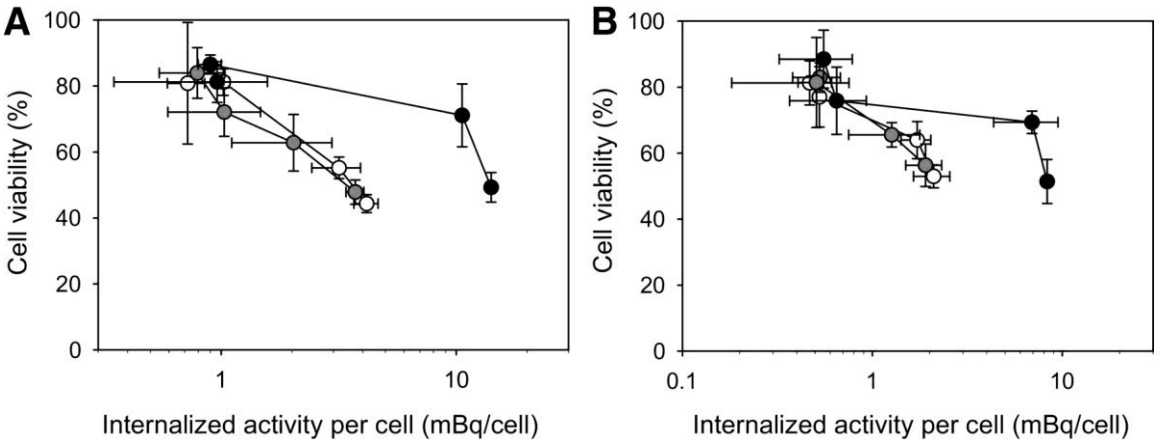


**Figure 3.6:** Viability of PSMA-positive HUVEC as a function of delivered radioactivity per cell mediated by the Ab-targeted radiolabeled vesicles (white symbols), the urea-based targeted radiolabeled vesicles (gray symbols), and radiolabeled antibody (black symbols), in static incubation conditions (A), and in the presence of a flow field (B).

*Intracellular Localization of Constructs*

Uptake of fluorescently-labeled, antibody- and urea-targeting liposomes resulted in punctate fluorescence regions within the cytoplasm and the perinuclear region of PSMA-expressing HUVEC (Figure 3.7A). In contrast, the PSMA-targeting antibody localized primarily around the plasma membrane and further away from the cell nucleus. Chlorpromazine, an inhibitor of clathrin-mediated endocytosis, did not affect cell uptake of any construct as seen under fluorescence microscopy and flow cytometry. Genistein, an inhibitor of caveolae-mediated endocytosis, decreased cellular uptake of all constructs as seen on flow cytometry results. Under fluorescence imaging, the presence of genistein resulted in localization of targeted liposome constructs on the cell's plasma membrane, suggesting successful ligand-receptor binding, but no endocytosis.

A quantitative analysis of the distance of fluorescence from the cell nucleus supports previous observation of the enhanced cytoplasmic and perinuclear localization of liposomal constructs over that of the antibody. Similarly, liposomes localized further

from the nucleus and around the plasma membrane in the presence of genistein (Figure 3.7B).

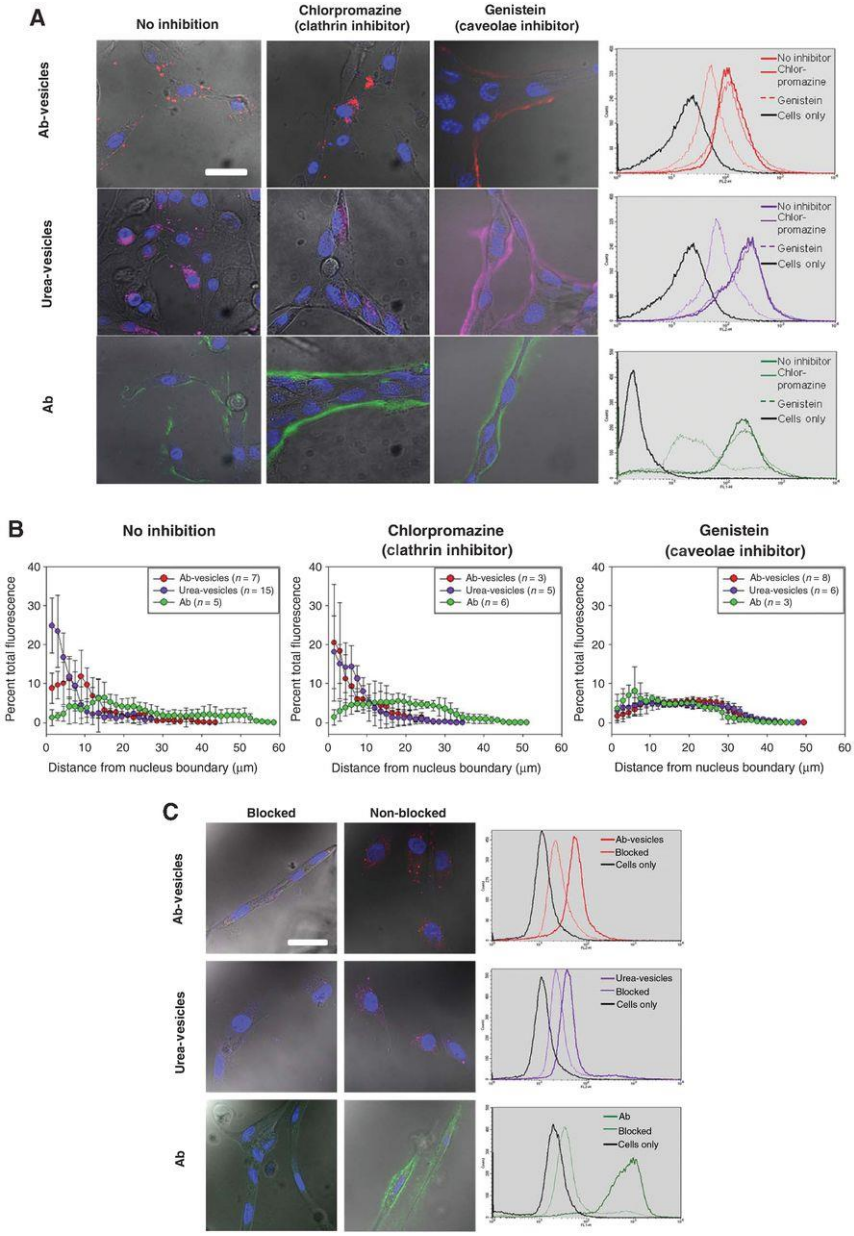


**Figure 3.7:** (A) intracellular spatial distribution (fused fluorescence and bright field images) and flow-cytometric shifts in the absence and presence of endocytosis inhibitors: first panel, antibody-liposomes (red); second panel, urea-liposomes (purple); third panel, fluorescent antibody (green), in PSMA+ HUVEC. Cell nuclei are stained in blue. Scale bar, 40 μm. (B) corresponding quantitative intracellular distributions of antibody-liposomes (red symbols), urea-liposomes (purple symbols), and the antibody (green symbols) in above incubating conditions. n indicates number of analyzed cells. Error bars, SD of the means of analyzed cells. (C) cell uptake (fused fluorescence and bright field images) and flow-cytometric shifts in the absence and presence of presaturation of

cells with the free PSMA antibody or the free lysine glutamate urea agent at 1,000× excess relative to cell receptors.

*Induction of γ-H2AX*

The number of fluorescent γ-H2AX foci, denoting double strand breaks in DNA, was counted within at least 50 cells treated with each of 3 targeted constructs. Cells treated with $^{225}$Ac antibodies had at most 25 γ-H2AX foci, whereas cells treated with either liposomal construct generated up to 40 – 50 foci (Figure 3.8).

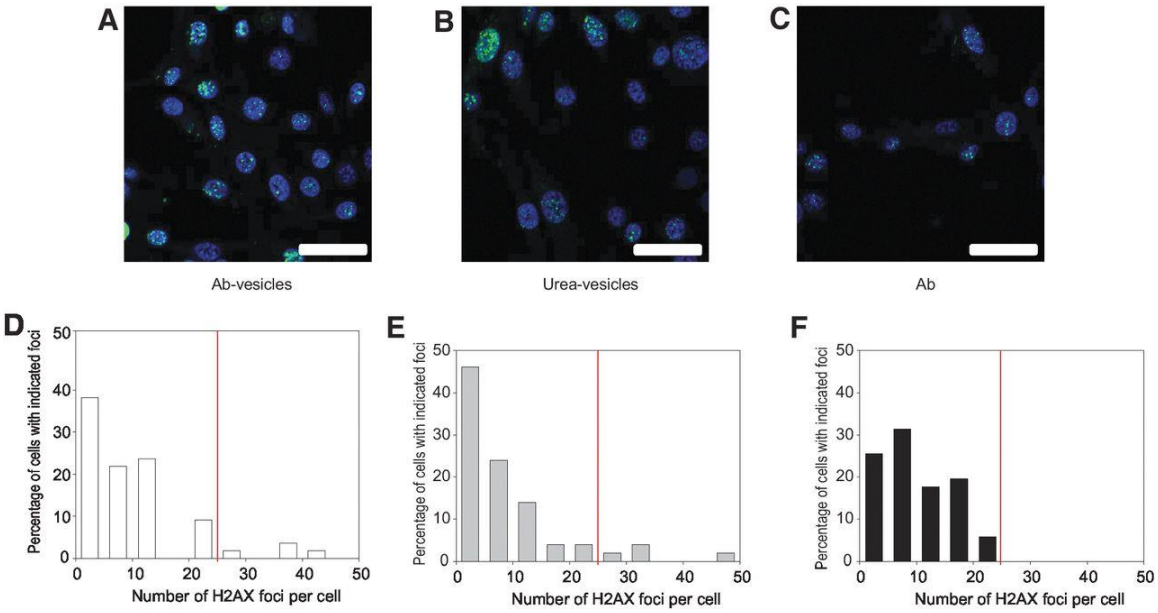


**Figure 3.8:** Characteristic images obtained by immunofluorescent staining of γ-H2AX foci (green) in cell nuclei (blue), and distribution of the number of foci per cell nucleus upon exposure to the antibody-liposomes (A), urea-liposomes (B), and the radiolabeled Ab (C). Corresponding distributions of γ-H2AX foci per cell for Ab-targeted vesicles (white bars; D), urea-based targeted vesicles (gray bars; E), and the antibody (black bars; F) were obtained by counting at least 50 cells per case. The red line serves as a threshold to indicate the maximum limit of foci mediated by the radiolabeled antibody. Scale bar, 40 μm.

## 3.4 Discussion

Our study demonstrated that by enhancing the cytoplasmic and perinuclear localization of $^{225}$Ac constructs closer to a cell nucleus, we can further improve the

already high cytotoxicity of delivered alpha particles. Our results show that per unit radioactivity delivered, liposomal constructs of $^{225}$Ac are up to three times more lethal than antibody constructs. The increase in killing efficacy per delivered radioactivity was correlated with an increased number of γ-H2AX foci on $^{225}$Ac-liposome-treated HUVEC and increased cytoplasmic/perinuclear localization. In contrast, treatment with $^{225}$Ac-antibodies results in localization near the plasma membrane, resulting in fewer γ-H2AX foci and more $^{225}$Ac per cell required for similar killing.

Enhancing the perinuclear localization of $^{225}$Ac effectively increases the solid angle of at least the first alpha-particle emission with respect to the nucleus, and thereby the overall probability of a nuclear hit as well as overall dosimetry of the cell nucleus. Microdosimetry modeling conducted with MIRDcell 2.0 software demonstrates the increased dose absorbed by the cell nucleus with perinuclear localization of $^{225}$Ac over cytoplasmic and plasma membrane localization.

*Future Studies*

Previously published work [52], which was also described in Chapter 2 of this dissertation, suggested that the choice of targeting ligand may affect therapeutic efficacy of $^{225}$Ac constructs. $^{225}$Ac-liposomes functionalized with anti-PSMA J591 antibody had similar overall efficacy with that of $^{225}$Ac-radiolabeled J591 antibody, both of which outperformed $^{225}$Ac-liposomes functionalized with the A10 aptamer, suggesting possible differences in intracellular trafficking or distribution with different targeting ligands. Therefore, several different targeting moieties may need to be tested to determine the best candidate.

Targeted therapies, particularly when used against cells with low target receptor expression, can be improved by reducing the dissociation constant $K_D$ (higher binding affinity) and increasing the specific activity of the radionuclide carrier (fewer non-radioactive but targeted constructs competing for a limited pool of receptors). PSMA receptor counting on induced HUVEC using the $^{111}$In-radiolabeled anti-PSMA antibody yielded a result of 52,000 receptors per HUVEC. This number of PSMA is low, especially when compared with the highly-expressing LnCaP cell line, which was previously reported to express $1.8 \times 10^5$ PSMA per cell, and measured at $(2.0 \pm 0.3) \times 10^5$ receptors per cell. The apparent $K_D$ of our $^{225}$Ac liposomal constructs may be potentially improved further by optimizing the density of conjugated ligands, or liposome diameter. Similar work targeting Human Epidermal Growth Factor 2 (HER2) receptor has already been published by our group and describes increasing ligand density on liposomes to improve targeting of low-expressing cells [61]. Increasing the specific activity of $^{225}$Ac-liposomes can be accomplished by increasing the initial radioactivity during liposome loading.

# CHAPTER 4: pH-TRIGGERED ACTINIUM-225 LIPOSOMES FOR SOLID TUMOR THERAPY

Note: data in this chapter was adapted from the following manuscript that has been submitted for publication:

1.) **Zhu C**, Holleran T, Linz T, Sempkowski M, Josefsson A, Rosen A, Howell R, Bruchertseifer F, Morgenstern A, Sofou S, Increased Interstitial Penetration of Highly-Diffusing α-Particle Emitters Delivered and Released by Tunable Liposomes Enhances Therapeutic Efficacy on Solid Tumor Analogues.

## 4.1 Introduction

Locally advanced and unresectable cancer characterized by a vascularized solid tumor remains a difficult-to-treat disease that has few therapy options and poor prognosis [1]. Barriers to successful therapy include poor drug uptake into the tumor and poor drug penetration throughout the tumor interstitium, resulting into heterogeneous drug distribution and low killing efficacy of unexposed cells [12, 62, 63].

Traditionally in radiation therapy, solid tumors are treated with beta-particle radionuclides, which emit particles that have tissue penetration ranging from 0.5 mm to 50 mm. The poor penetration of drug delivery carriers into the solid tumor space is then overcome by the long-range emissions that can deliver therapeutic radiation to the core of the tumor [8, 14]. This approach however, has several drawbacks. First, the long-range beta emissions subject large volumes of surrounding healthy tissues to radiation, resulting in toxicities that ultimately limit the administered dose from a patient safety perspective [64]. Second, low LET radiation like beta-emitters (0.2 keV/μm) inflict mostly single-

strand DNA breaks and rely on secondary mechanisms such as the creation of reactive oxygen species (ROS) via ionizing radiation to result in cell kill [8]. Given the hypoxic nature of many solid tumors, a reliance on ROS for therapeutic efficacy is far from optimal.

Alpha-particle emitters are typically not considered as agents for solid tumor therapy because their short-range emissions (50 – 90 μm) do not overcome the poor penetration of drug carriers into the tumor interstitium. However, alpha-particles have very high LET (80 – 120 keV/ μm) that result in oxygen-independent killing via double strand DNA breaks. The short-range of alpha particles limits the volume of surrounding healthy tissue irradiation, and the oxygen-independent killing is unaffected by hypoxic microenvironments. The major barrier to success to alpha-particle therapy of solid tumors is the poor penetration of the therapeutic throughout the tumor interstitium.

The drug penetration problem is not unique to alpha-particle emitters, and has been encountered in chemotherapies as well. Several strategies exist to improve the intra-tumor drug distribution, which includes pH-responsive liposomes that retain chemotherapeutics at pH 7.4 (e.g. while in circulation), and release their highly diffusive contents at pH 6.0 – 6.8 (experienced within the acidic tumor interstitium) that can spread throughout the tumor. Such pH-responsive systems have been already been evaluated for delivery of doxorubicin [34, 42].

We hypothesize that by using a similar approach, wherein pH-responsive liposomes loaded with the alpha particle emitter $^{225}$Ac, we can improve the intra-tumoral distribution of alpha-particle irradiation and therefore its overall killing efficacy. We tested our hypothesis by treating *in vitro* analogues of solid tumors (multicellular

spheroids) with $^{225}$Ac-liposomes triggered to release their contents at pH 6.0 – 6.8 and compare to $^{225}$Ac-radiolabeled antibodies. We evaluate nanocarrier and $^{225}$Ac penetration into spheroids, as well as the spheroids' pH gradients. Selected constructs were then tested *in vivo* within murine models bearing orthotopic xenograft tumors implanted within their mammary fat pad.

## 4.2 Materials and Methods

*Liposome Preparation*

The following lipids were used for liposome preparation: 1,2-dihenarachidoyl-sn-glycero-3-phosphocholine (21PC), 1,2-distearoyl-sn-glycero-3-phosphate (Sodium Salt; DSPA), 1,2-distearoyl-sn-glycero-3-phosphoethanolamine-N-[Methoxy(Polyethylene glycol)-2000] (Ammonium Salt; DSPE-PEG2000), 1,2-distearoyl-sn-glycero-3-phosphoethanolamine-N-[PDP (Polyethylene Glycol) 2000] (Ammonium Salt; DSPE-PEG-PDP), 1,2-dipalmitoyl-sn-glycero-3-phosphoethanolamine-N-(LissamineRhodamine B Sulfonyl) (Ammonium Salt; DPPE-Rhodamine), and cholesterol (chol).

Conventional liposomes (non-pH releasing liposomes) designed to stably retain their contents irrespective of external pH were composed of a 66.0:28.3:4.7:1.0 mole ratio of 21PC:chol:DSPE-PEG2000:DPPE-Rhodamine. Liposomes triggered to release under acidic pH (pH-releasing liposomes) were composed of 53.7:23.0:9.5:13:0.8 mole ratio of 21PC:DSPA:chol:DSPE-PEG2000:DPPE-Rhodamine. All components were dissolved in chloroform or a chloroform-methanol mixture and combined in a round bottom flask. Lipid mixtures were dried under vacuum and rotation at 55°C followed by

further drying under $N_2$ gas to yield a thin film. Lipids were hydrated in citrate buffer (140 mM citrate, 5 mg/mL 1,4,7,10-tetraazacyclododecane-1,4,7,10-tetraacetic acid (DOTA), 2.1 mg/mL ascorbic acid, pH 5.0) and incubated at 55°C for 2 hours. The suspension was extruded 21 times through two polycarbonate membranes with 100 nm pore diameter, and eluted through a Sepharose 4B column with HEPES buffer (20 mM HEPES, 250 mM sucrose, pH 7.4). Liposome size and polydispersity index were determined using a Zetasizer NanoSeries.

Loading of $^{225}$Ac was accomplished as previously described in literature[36, 52] and Chapters 2 and 3 of this dissertation. Briefly, 80 µL of a mixture containing 30 µL of $^{225}$Ac dissolved in 0.03 mM HCl and 50 µL of 0.37 mg/mL calcium ionophore A23187 in a 1:1 mixture of metal-free water and ethanol to 1 mL of liposomes (5 mM total lipid). After incubating the liposome-$^{225}$Ac-A23187 mixture for 1 hour at 80 °C, 50 µL of DTPA was added to chelate unentrapped $^{225}$Ac, and the entire volume was passed through a Sephadex G50 column eluted with phosphate buffered saline (PBS) + 1 mM Ethylenediaminetetraacetic acid (EDTA) to separate liposomes from un-encapsulated $^{225}$Ac.

The form of released radioactivity from liposomes ($^{225}$Ac, $^{225}$Ac-DOTA, $^{225}$Ac-ionophore complex) was evaluated are follows. The $^{225}$Ac-DOTA chelate was selectively separated at ~100% yield from the other two forms by TLC using 10 mM sodium hydroxide with 9% sodium chloride (wt/wt) in metal free water as the mobile phase [17]. The 225Ac-ionophore complex was selectively separated at almost 60% yield from the other two forms by extraction in an organic phase (7:3 v/v Toluene:n-Butanol) at 1-to-2 aqueous-to-organic phase volume ratio.

*Antibody Radiolabeling*

Antibody radiolabeling was performed as previously described in literature[37] and differently than described in Chapters 2 and 3 of this dissertation. Briefly, an isothiocyanate-functionalized metal chelators (either DTPA or DOTA) was added to trastuzumab or IgG1κ isotype control antibodies at a 15:1 mole ratio in 1 M carbonate buffer (pH 9.0) and incubated overnight with shaking. Antibody-chelator conjugates were separated from unreacted metal chelators by eluting the mixture through a 10-DG column with 1 M acetate buffer, pH 7.4 (DTPA-antibodies) or 0.1 M tris buffer, pH 9.0 (DOTA-antibodies). Radionuclides (either $^{225}$Ac or $^{111}$In) dissolved in 0.2 M HCl was added to the mixture, which was heated to 37°C for 1 hour. Free radionuclide was removed from radiolabeled antibodies by first adding 50 µL of 10 mM EDTA ($^{111}$In-antibodies) or DTPA ($^{225}$Ac-antibodies) to the mixture, then eluting it through a 10-DG column with PBS (pH 7.4) + 1 mM EDTA. Radiochemical purity of the final product was assessed via instant thin layer chromatography (iTLC) using 10 mM EDTA as the mobile phase.

*Nanocarrier Retention of Actinium-225*

Nanocarrier (liposome or antibody) retention of $^{225}$Ac was determined by incubating $^{225}$Ac-loaded carrier in HybriCare cell culture media supplemented with 10% fetal bovine serum (FBS). At pre-determined time points, a 1 mL aliquot was added with 50 µL of 10 mM DTPA and eluted with PBS through either a Sephadex G-50 (liposomes) or 10-DG (antibodies) SEC column. The percentage of $^{225}$Ac retained was calculated by comparing Bi-213 γ-emissions before and >5 hrs after SEC.

*Radiosensitivity of Cells*

Suspended cells were irradiated either with Cs-137 external beam irradiator (2, 4, 6, 8, 10, 12 Gy), or with $^{225}$Ac-IgG1κ isotype control antibody for 6 hours (7.4, 14.8, 29.6, 59.2, or 74 kBq/mL) and plated for colony survival or MTT viability. For colonies, cells were incubated for 10 doubling times, washed with PBS, and stained with 0.5% crystal violet and 6% glutaraldehyde in water for 30 minutes. Colony plates were then de-stained with 3 washes of water. Clusters with at least 50 cells were considered as viable colonies, each of which originated from one viable cell at beginning of the incubation time. For MTT, cells were incubated for 2 doubling times and then exposed to MTT dye as an assessment of overall mitochondrial activity.

*Cell Culture and Spheroid Initiation*

BT-474 and MDA-MB-231 cells were maintained in HybriCare and EMEM cell culture media, respectively, supplemented with 10% FBS, 100 units/mL penicillin, and 100 µg/mL streptomycin at 37°C, 5% $CO_2$. Spheroids were initiated by seeding 400 (BT-474) or 125 (MDA-MB-231) cells/well into polyHEMA-coated 96-well plates with U-shaped wells, centrifuged for 5 minutes at 500 x gravity, and incubated until spheroids grew to appropriate size (typically at least one week). MDA-MB-231 spheroids were initiated in the presence of 2.5% Matrigel™ within culture media.

*Interstitial pH-Gradients*

The interstitial spheroid pH gradient was determined by incubating spheroids overnight with SNARF-4F pH-responsive fluorophore, moving the spheroids to fresh media, and acquiring optical sections through the spheroid equator using laser scanning confocal microscopy. The ratio of fluorescence (640nm/580nm) was used to quantitatively determine the pH in the spheroid interstitium.

*Spheroid Treatment*

Spheroids were incubated for six hours with cell culture media containing liposomes (0.1 μmol lipids) or 10 μg/mL trastuzumab at a final radioactivity of 18.5, 3.7, or 0.37 kBq/mL $^{225}$Ac. The following controls were used: 1.) $^{225}$Ac-labeled IgG1κ isotype control, 2.) spheroids incubated with non-radioactive nanocarriers (0.1 μmol liposomes or 10 μg/mL trastuzumab), and 3.) no treatment. Following treatment, spheroids were washed and then placed in non-radioactive media. Spheroid volume was tracked up to 29 days, until the untreated population stopped growing, or until spheroid disaggregation/cell death. Volume was determined as $V = (1/6)*\pi*(a*b^2)$, where a and b refer to the major and minor axes, respectively of the assumed ellipsoid.

MDA-MB-231 spheroids, due to initiation in Matrigel™, were plated in wells following treatment with $^{225}$Ac constructs to allow outgrowth of viable cells. After 10 doubling times, treated spheroids were stained with Hoechst 33342 and imaged under fluorescence microscopy.

*Nanocarrier and $^{225}$Ac Penetration into Spheroids*

To determine the intra-spheroid distribution of nanocarriers, spheroids were incubated with non-radioactive, fluorescently-labeled trastuzumab or liposomes. Uptake and clearance of liposomal contents was also evaluated using non-fluorescent liposomes encapsulating a non-self-quenching concentration of the fluorophore calcein (2.5 mM). Following penetration of nanocarriers for pre-determined timepoints, spheroids were either washed and incubated for additional clearance timepoints in fresh media prior to freezing and cryosectioning, or immediately placed into OCT, frozen, and sliced. 20 µm-thick sections were evaluated under fluorescence microscopy. The concentration of nanocarrier as a function of spheroid radial position was determined using an image-processing erosion algorithm that draws concentric circles from the edge of the spheroid into the core. Calibration curves were generated by measuring the intensities of serial dilutions of known construct concentrations in a cuvette with 20 µm pathlength.

To determine the distribution of $^{225}$Ac radioactivity, spheroids were incubated in the presence of $^{225}$Ac-constructs for 6 hours, washed, and then frozen within OCT. Spheroids were then sectioned at 8 µm thickness and placed on a sheet composed of a Zinc-Sulfur-Silver scintillation material that emits photons when exposed to alpha particles. Radioactivity within spheroids were determined under alpha-camera as previously described [65, 66]. Briefly, The α-Camera calibration coefficient y (Bq/(pixel intensity unit-hours)) for equilibrium 225Ac expressed as a function of the image pixel size x (µm) was determined by measuring the activity (Bq) of the imaged sample in a gamma well counter (Perkin-Elmer 2470 WIZARD2® Automatic Gamma Counter, MA, USA) using the 400 to 480 keV energy window for $^{213}$Bi (440.6 keV and yield 26.1%). A

region of interest (ROI) was drawn around the tissue in the α-Camera image to determine the pixel intensity unit per hour of acquisition. The plotted experimental data was fitted with a second-order polynomial expression (R2 = 0.9954), y=0.0241*x^2+0.9351*x-0.4708. The average activities of $^{225}$Ac as a function of spheroid radial position were determined using the eroding algorithm described above (of 11-16 μm thickness rings).

As a secondary measure of $^{225}$Ac penetration through the interstitial space, spheroids were treated with $^{225}$Ac constructs (radiolabeled non-pH releasing liposomes, pH-releasing liposomes, and trastuzumab antibodies) for 6 hours, washed, and further incubated in non-radioactive medium for 1 hour to induce γH2AX signal within the cells. Spheroids were then washed in PBS, fixed in 10% formalin for 1 hour, and incubated in 30% sucrose overnight. Spheroids were then mounted in OCT gel, frozen, and sectioned at 20 μm thickness. Spheroid slices were placed on a poly-lysine coated cationic slide, washed with PBS, and permeabilized with ice-cold 90% methanol in water for 10 minutes. Following permeabilization, slices were washed with PBS to remove residual methanol, and blocked with 5% bovine serum albumin (BSA) in PBS for 1 hour at room temperature. Anti-phospho-H2AX primary antibody dissolved in 1% BSA/PBS (Clone JBW301, 2 μg/mL) was placed on the samples overnight at 4°C to probe for the presence of γH2AX, an indicator of dsDNA breaks. Following primary antibody incubation, samples were washed 5 times with 0.1% Tween20 in PBS and incubated with 4 μg/mL AlexaFluor-555-goat anti-mouse IgG1 overnight, after which samples were washed again 5 times with 0.1% Tween20 in PBS. Spheroid slices were imaged under a fluorescence microscope in the red filter channel to visualize γH2AX location.

*In Vivo Evaluation*

The maximum tolerated dose (MTD) of $^{225}$Ac-radiolabeled trastuzumab, IgG1κ isotype control antibodies, non-pH releasing liposomes, and pH-releasing liposomes was determined by injecting healthy athymic nude mice weighing approximately 20 grams with varying doses of radioactivity (100, 250, 400, 500, and 900 nCi per mouse). MTD was defined as the maximum dose at which no mouse died or required euthanasia per Institutional Animal Care and Use Committee protocol (IACUC). Animals were euthanized if they were exhibiting signs of severe distress (>10% weight reduction, unresponsive to external stimuli, difficulty breathing, loss of mobility, etc.). Doses of $^{225}$Ac constructs were administered via retro-orbital injection. Orthotopic xenograft tumors were implanted via mammary fat pad injection. A small incision was made on each mouse, allowing injection of 2 million MDA-MB-231 cells suspended in serum-free cell culture media into the secondary mammary fat pad on the right side of the animal. $^{225}$Ac therapy or saline was administered once tumors had reached 100 mm$^3$ in volume. Animal weight, tumor volume, and overall survival were tracked. Per IACUC protocol, animals were euthanized if they met conditions for euthanasia during MTD studies, or if tumors exceeded 10% of the overall weight of the mouse. Survival statistics were analyzed using Mann-Whitney statistical testing.

## 4.3 Results

*Nanocarrier Characterization*

Both conventional and pH-triggered liposomes exhibited stable retention (approximately 80%) of encapsulated $^{225}$Ac after 24 hours incubation in 10% serum-

supplemented media at pH 7.4 (Figure 4.1). Decreasing pH to slightly acidic ranges (6.0 – 6.8) resulted in lower retention in pH-triggered liposomes (49 – 66% after 24 hours), while having no effect on stability of conventional liposomes. The size of liposomes was estimated by dynamic light scattering to be 114 ± 13 nm (PDI: 0.08 ± 0.03). Radiolabeling of trastuzumab and IgG1κ isotype control antibodies with $^{225}$Ac using a one-step protocol resulted in radiolabeling efficiencies ranging from 70.1 – 92.3% and radiochemical purities of >95% by iTLC. Antibody-DOTA conjugates retained 86.1% of initial $^{225}$Ac after 6 hours incubation in 10% serum-supplemented media at pH 7.4.

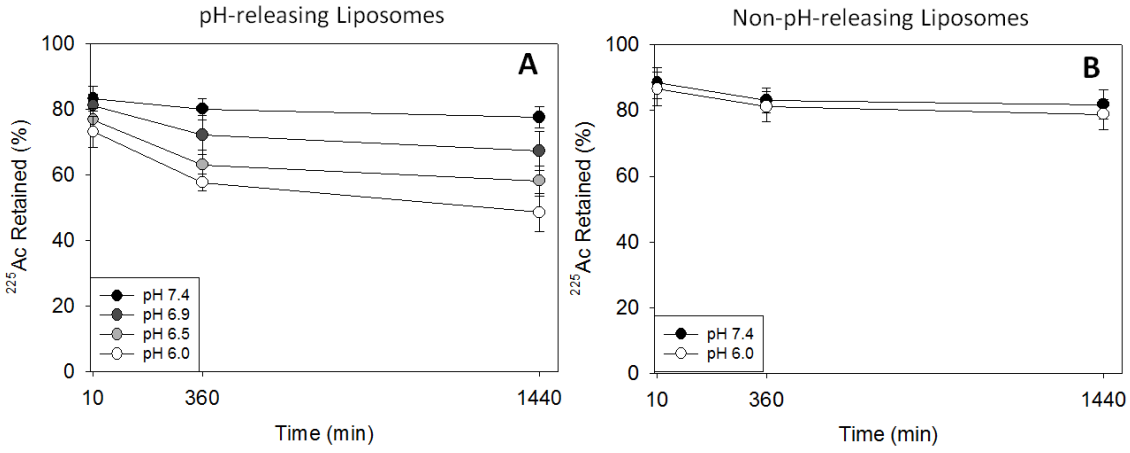


**Figure 4.1**. Retention of radioactive contents as a function of pH over time by (A) pH-sensitive and (B) non pH-sensitive liposomes. Lipospomes were incubated in serum supplemented media at 37$^{o}$C. Errors correspond to standard deviations of repeated measurements (n = 3 independent liposome preparations, 2 measurements per preparation). Lines are guides to the eye.

*Cell and Multicellular Spheroid Characterization*

The BT-474 and MDA-MB-231 cell lines were chosen to broadly represent cases of varying HER2/*neu* expression, which in this scenario was our target receptor. Analysis using immunohistochemistry classified BT-474 as a HER2 overexpressing cell line. MDA-MB-231, as a triple negative breast cancer line, expressed very low amounts of

HER2. Our studies using $^{111}$In-radiolabeled trastuzumab quantified the HER2 expression levels of BT-474 and MDA-MB-231 monolayers at $1.3 \pm 0.1 \times 10^6$ and $8.3 \pm 0.8 \times 10^5$ HER2 receptors per cell, respectively (Figure 4.2). Formation of either cell type into spheroids affected their HER2 expression (Figure 4.3). Flow cytometry analysis of cells typsinized from monolayers, 200 μm spheroids, and 400 μm spheroids and probed with fluorescein-labeled trastuzumab demonstrated a decrease in HER2 expression in the larger spheroids relative to monolayers and smaller spheroids.

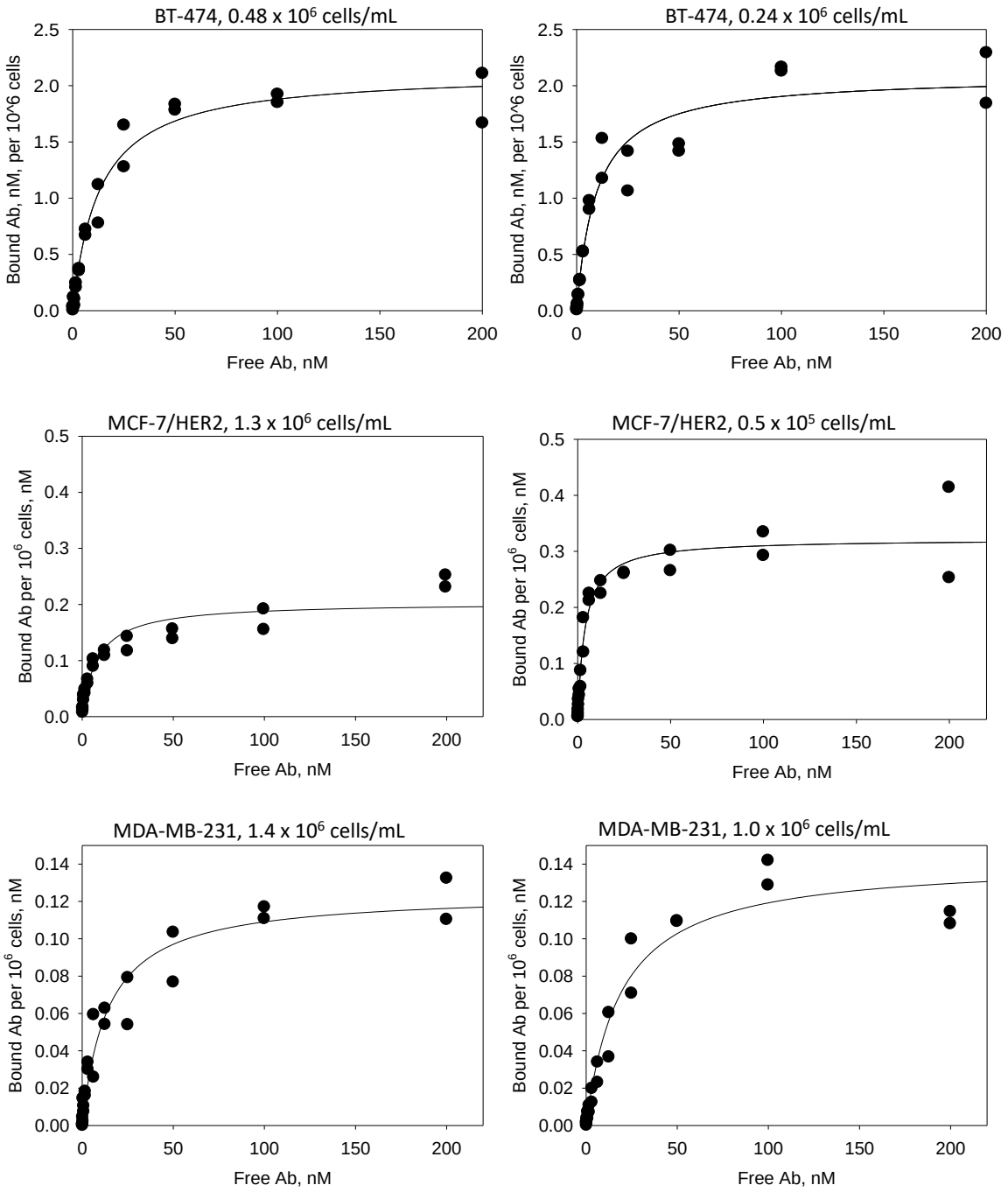


**Figure 4.2**. Binding curves of $^{111}$In-trastuzumab with the cell lines BT-474 (HER2-overexpressing), MCF-7/HER2 (HER2-expressing), and MDA-MB-231 (HER2-negative).

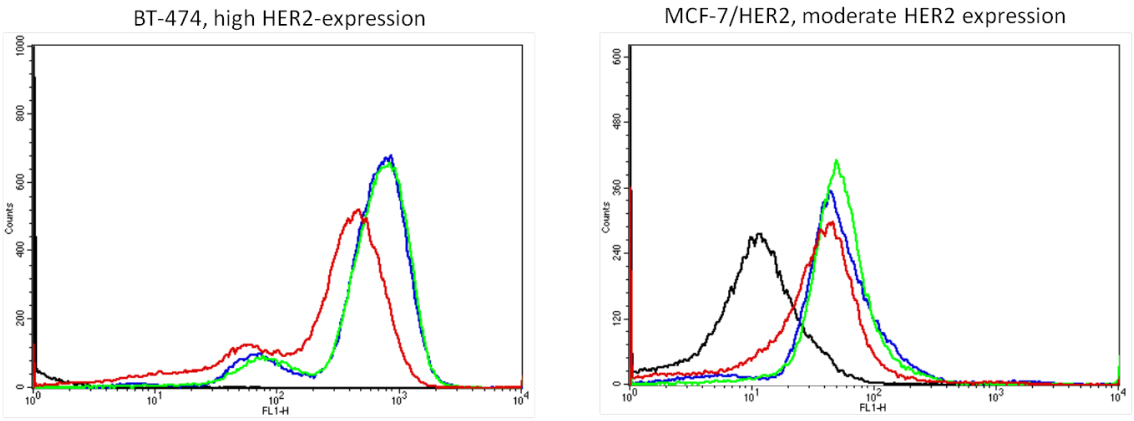


**Figure 4.3**. Fluorescence intensity shift by flow cytometry of HER2-expressing cells extracted from cell monolayers and from multicellular spheroids. Black line: cells only; green line: cell monolayers; blue line: 200 µm-in-diameter spheroids; red line: 400 µm-in-diameter spheroids.

The interstitial regions of spheroids formed with BT-474 and MDA-MB-231 cells all exhibited some degree of acidification (Figure 4.4). In general, spheroids at both 200 and 400 µm diameter acidified to pH 6.0 – 6.4 within the spheroid core from a near-neutral pH at the periphery.

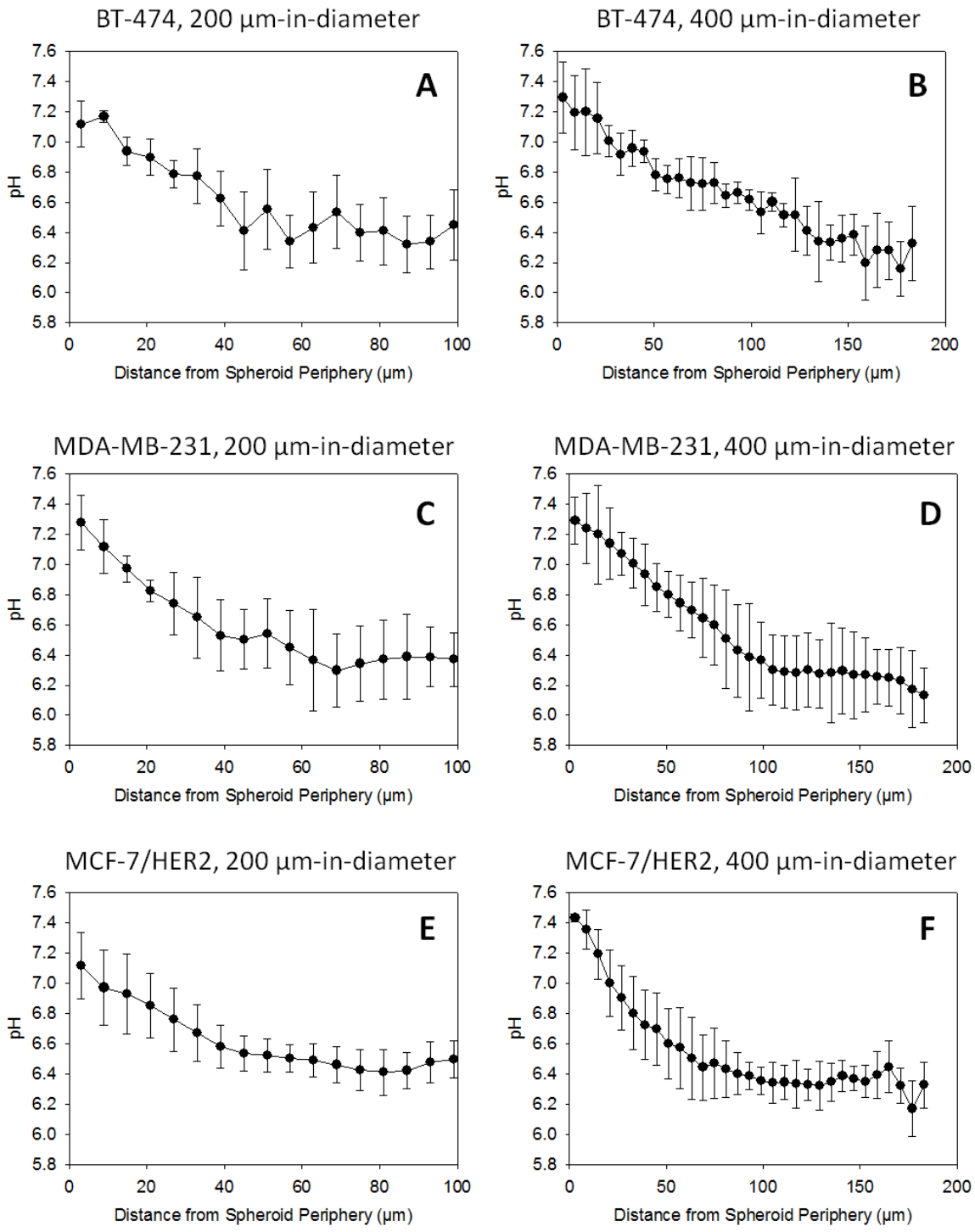


**Figure 4.4**. Interstitial pH gradients in 200 µm (left panel) and 400 µm (right panel) in-diameter spheroids measured using a membrane impermeant pH-sensitive fluorophore. (A, B) BT-474, (C, D) MDA-MB-231, (E, F) MCF-7/HER2. Error bars correspond to standard deviations from triplicate repeated measurements (n = 3 spheroids).

*Nanocarrier Uptake and Clearance from Spheroids*

Both non-pH releasing and pH-releasing liposomes exhibited similar uptake into, and clearance from both spheroid types (BT-474 and MDA-MB-231) and sizes (200 and 400 μm). Fluorescent liposomes were observed at a depth of roughly 30 and 50 μm into spheroids of 200 and 400 μm diameter, respectively, after 6 hours of incubation (Figure 4.5). Removal of the spheroids from liposome-containing medium into fresh medium without liposomes resulted in rapid decrease of fluorescence signal from the spheroids and a near-absence of liposomes after 4 hours of clearance time (Figure 4.6). BT-474 spheroids exhibited very high uptake of fluorescein-labeled trastuzumab at the spheroid periphery, presumably due to target receptor expression, while MDA-MB-231 spheroids exhibited little uptake. Antibodies cleared at a slower rate and were still present within BT-474 spheroids after 4 hours incubation in fresh medium.

Contrary to the interstitial spatiotemporal profiles of both pH- and non-pH-responsive liposomes, the uptake and clearance of their contents through the spheroids' interstitium exhibited different profiles. When delivered via pH-responsive liposomes, calcein was present throughout the entire volume of the spheroid after 6 hours of uptake. The calcein uptake of spheroids incubated with non-pH-releasing liposomes on the other hand, was very similar to that when fluorescently monitoring only the nanocarrier, suggesting that no significant content release occured (Figure 4.7, 4.8).

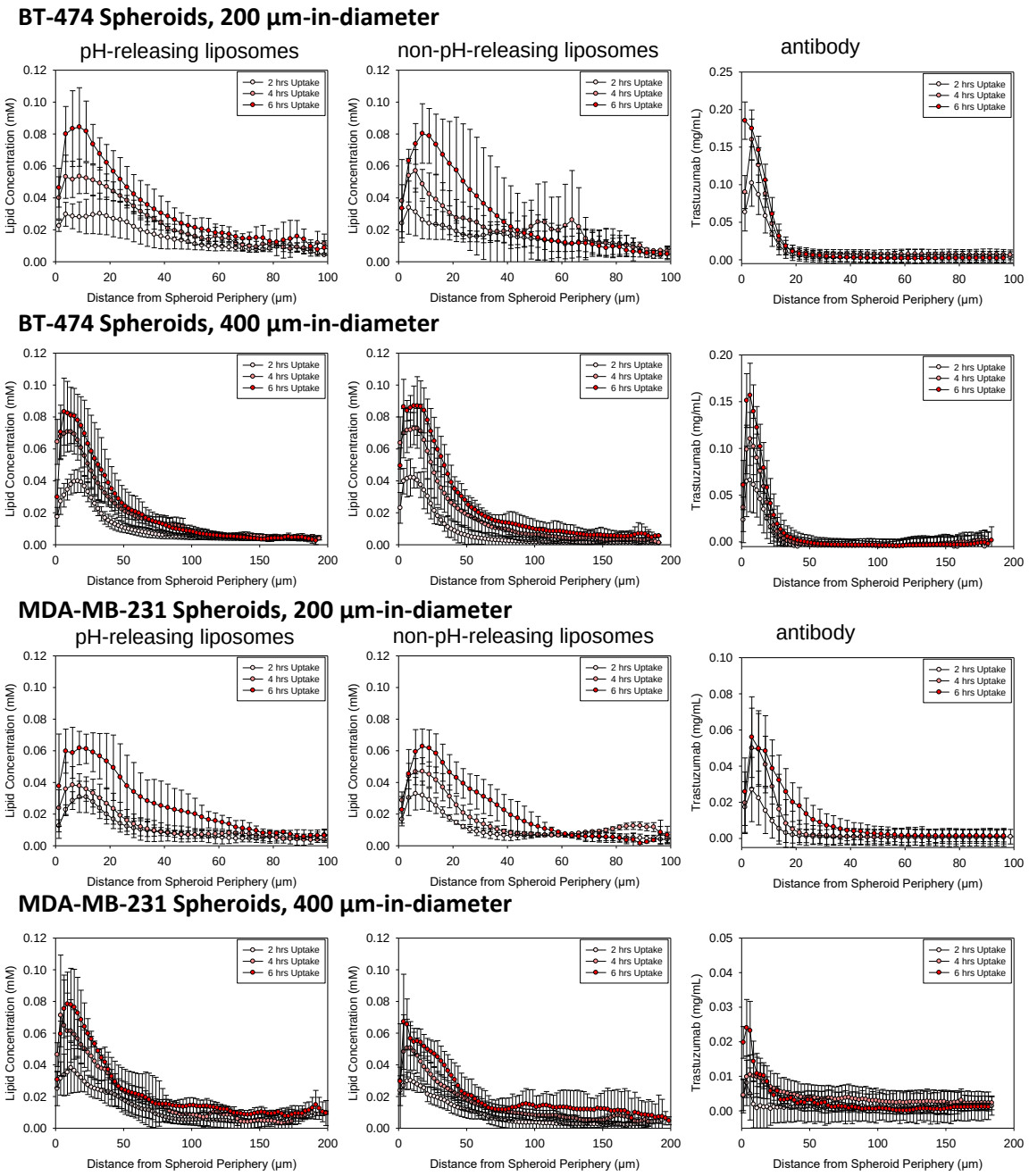


**Figure 4.5.** Uptake profiles of fluorescent pH-releasing liposomes (left column), non-pH-releasing liposomes (center column), and trastuzumab (right column).

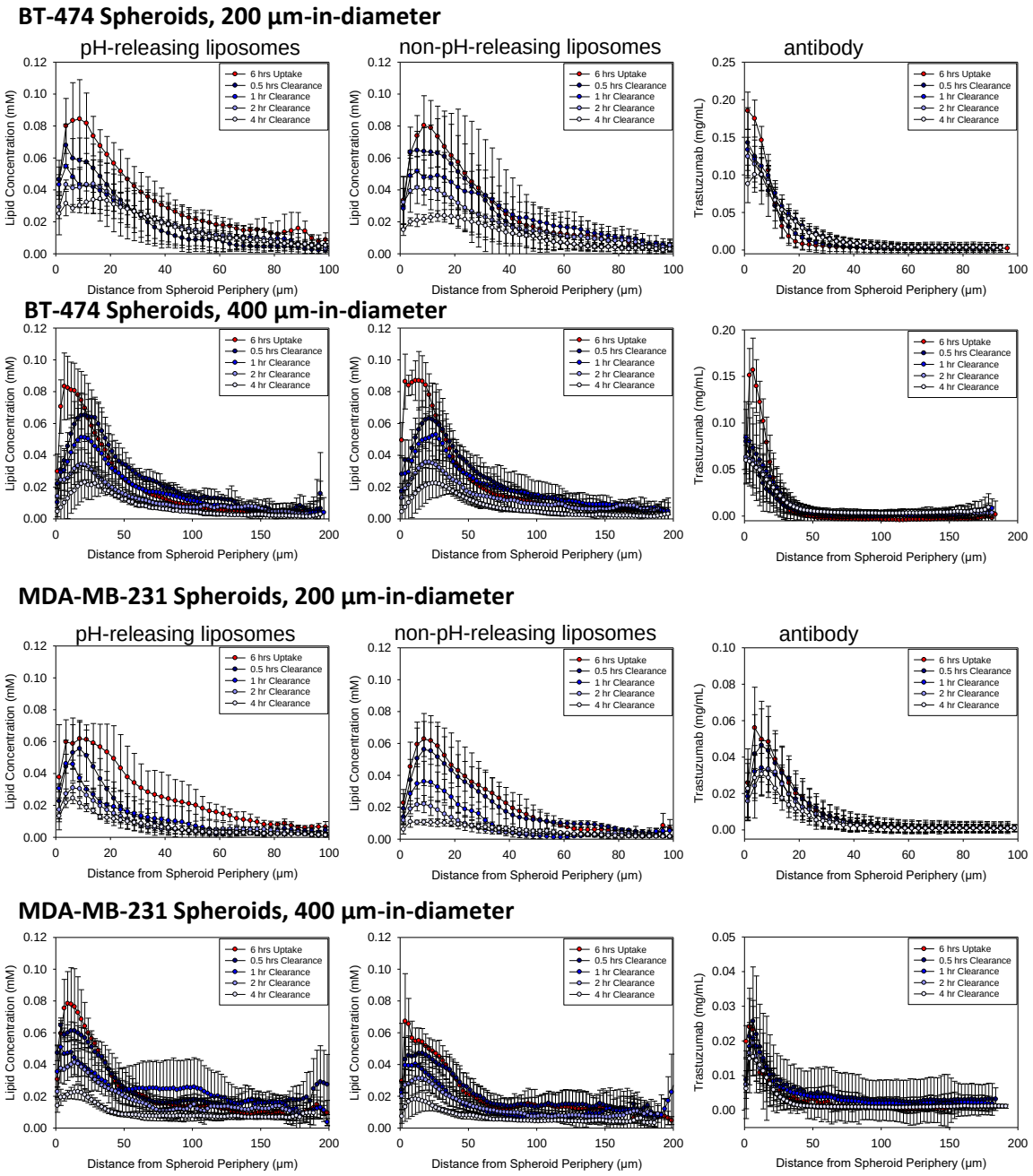


**Figure 4.6.** Clearance profiles in HER2 positive BT474 spheroids of 200 µm (top row) and 400 µm diameter (bottom row) of fluorescent pH-releasing liposomes (left column), non-pH-releasing liposomes (center column), and trastuzumab (right column).

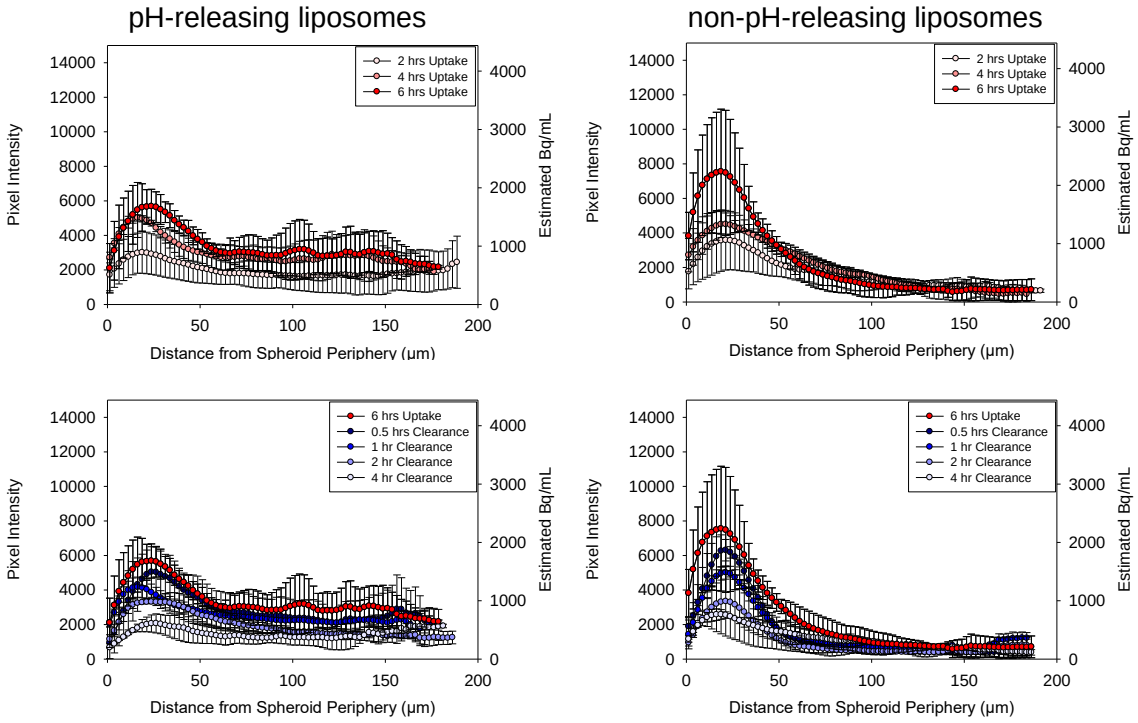


**Figure 4.7:** Uptake (top row) and clearance (bottom row) of liposomal contents delivered by pH- and non-pH-releasing liposomes (left and right column, respectively) onto BT-474 spheroids.

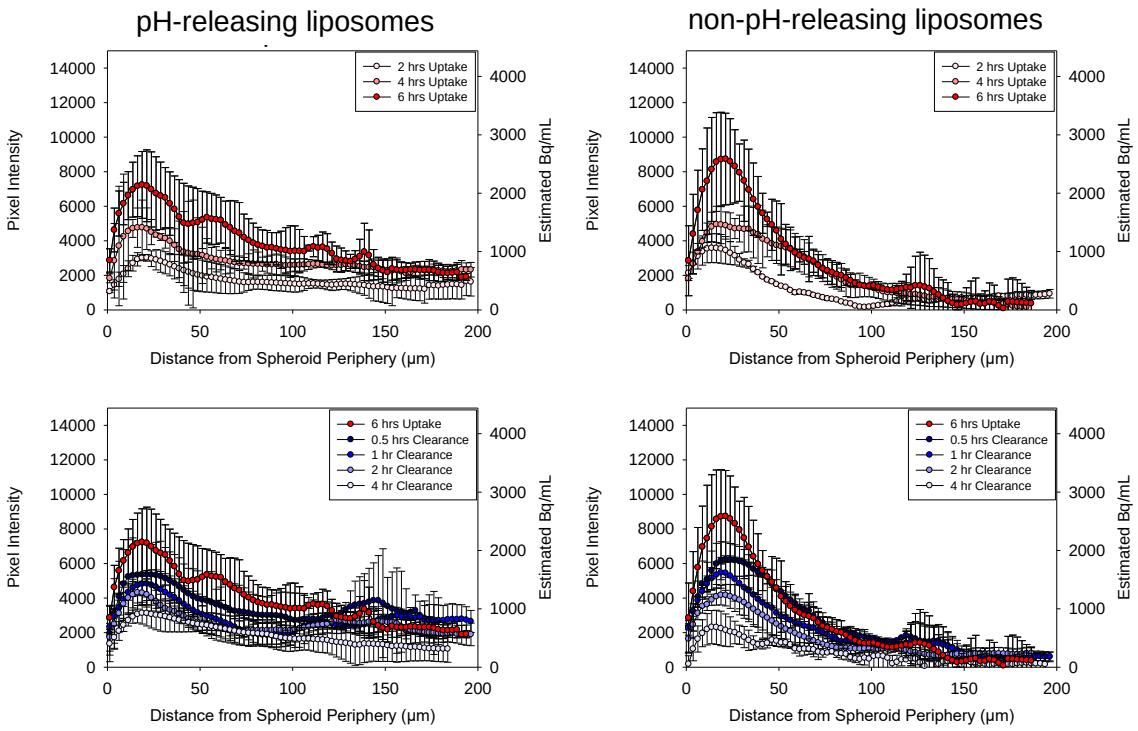


**Figure 4.8.** Uptake (top row) and clearance (bottom row) of liposomal contents delivered by pH- and non-pH-releasing liposomes (left and right column, respectively) onto MDA-MB-231 spheroids.

*Therapeutic Efficacy of $^{225}$Ac constructs*

On 200 μm-in-diameter BT474 spheroids, $^{225}$Ac-trastuzumab at 18.5 kBq/mL dose exhibited the highest efficacy followed by pH-releasing liposomes loaded with $^{225}$Ac while $^{225}$Ac-loaded non-pH releasing liposomes and $^{225}$Ac-IgG1κ isotype control antibodies merely delayed and reduced spheroid growth (Figure 4.9A). This overall efficacy trend was also observed at the intermediate dose of 3.7 kBq/mL (Figure 4.9B). At the lowest activity level of 0.37 kBq/mL $^{225}$Ac, all constructs exhibited minimal effect on spheroid growth (Figure 4.9C).

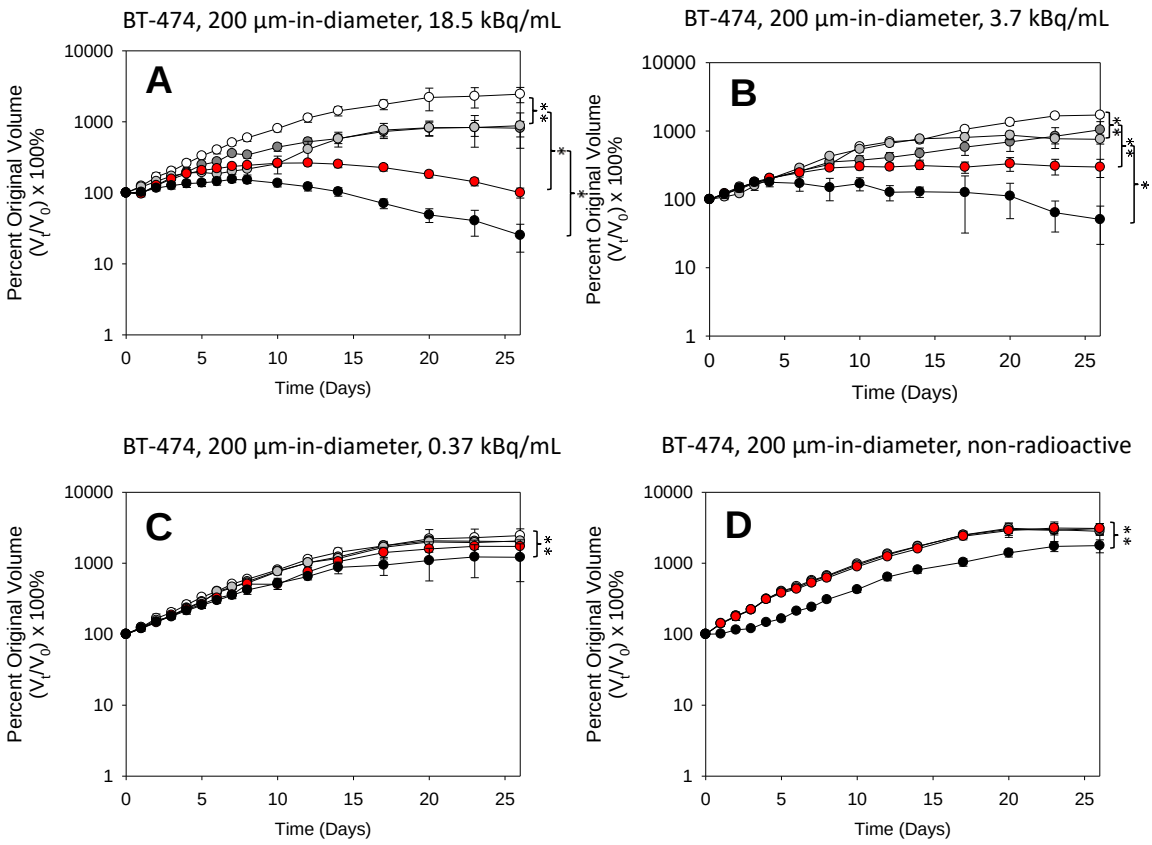


**Figure 4.9.** Efficacy of $^{225}$Ac constructs on 200 µm-in-diameter BT-474 spheroids. Spheroids were treated at (A) 18.5, (B) 3.7, (C) 0.37, or (D), 0 kBq/mL radioactivity in the form of non-pH-responsive liposomes (grey symbols), radiolabeled trastuzumab (black symbols), radiolabeled isotype control antibody (dark grey symbols), or pH-responsive liposomes (red symbols). White symbols denote media-only negative control and are always non-radioactive. Double asterisks denote $P < 0.05$, while single asterisk denotes $P < 0.01$.

Interestingly, on 400 µm BT474 spheroids, $^{225}$Ac-loaded pH-releasing liposomes exhibited greater efficacy than $^{225}$Ac-trastuzumab at both 18.5 and 3.7 kBq/mL activity levels (Figure 4.10), a trend that was not observed at the smaller 200 µm-in-diameter spheroid size. Similarly to the results obtained on 200 µm spheroids, the lowest radioactivity level of 0.37 kBq/mL had little effect on 400 µm spheroids (Figure 4.10).

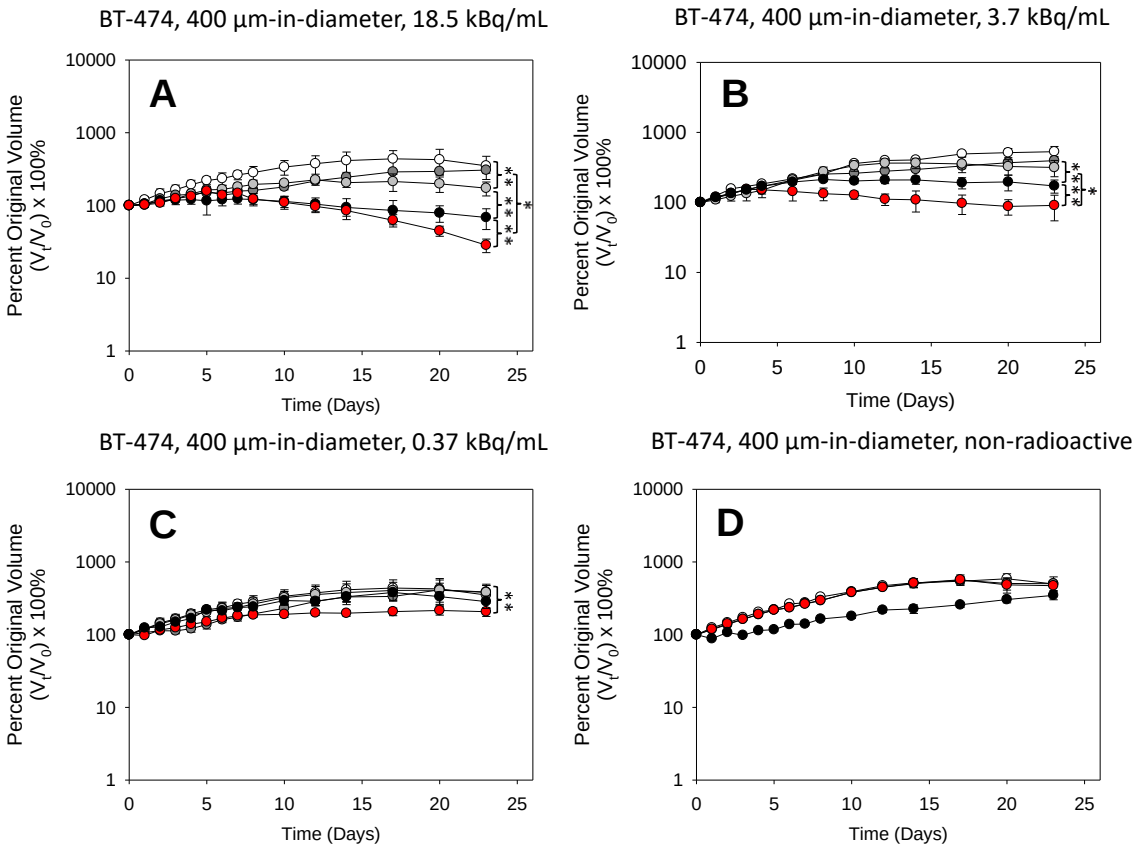


**Figure 4.10.** Efficacy of $^{225}$Ac constructs on 400 µm-in-diameter BT-474 spheroids. Spheroids were treated at (A) 18.5, (B) 3.7, (C) 0.37, or (D), 0 kBq/mL radioactivity in the form of non-pH-responsive liposomes (grey symbols), radiolabeled trastuzumab (black symbols), radiolabeled isotype control antibody (dark grey symbols), or pH-responsive liposomes (red symbols). White symbols denote media-only negative control and are always non-radioactive. Double asterisks denote $P < 0.05$, while single asterisk denotes $P < 0.01$.

Actinium-225-labeled trastuzumab was ineffective at treating MDA-MB-231 spheroids that exhibited very low target receptor expression, and showed similar efficacy profiles to that of $^{225}$Ac-IgG1κ isotype control antibodies at the same dose, whereas $^{225}$Ac-loaded pH-releasing liposomes at 18.5 and 3.7 kBq/mL activity levels exhibited the best therapeutic efficacy at both sizes of MDA-MB-231 spheroids (Figure 4.11, 4.12). Actinium-225-loaded non-pH releasing liposomes, as was observed on BT474 spheroids, was only effective in slowing the growth of MDA-MB-231 spheroids.

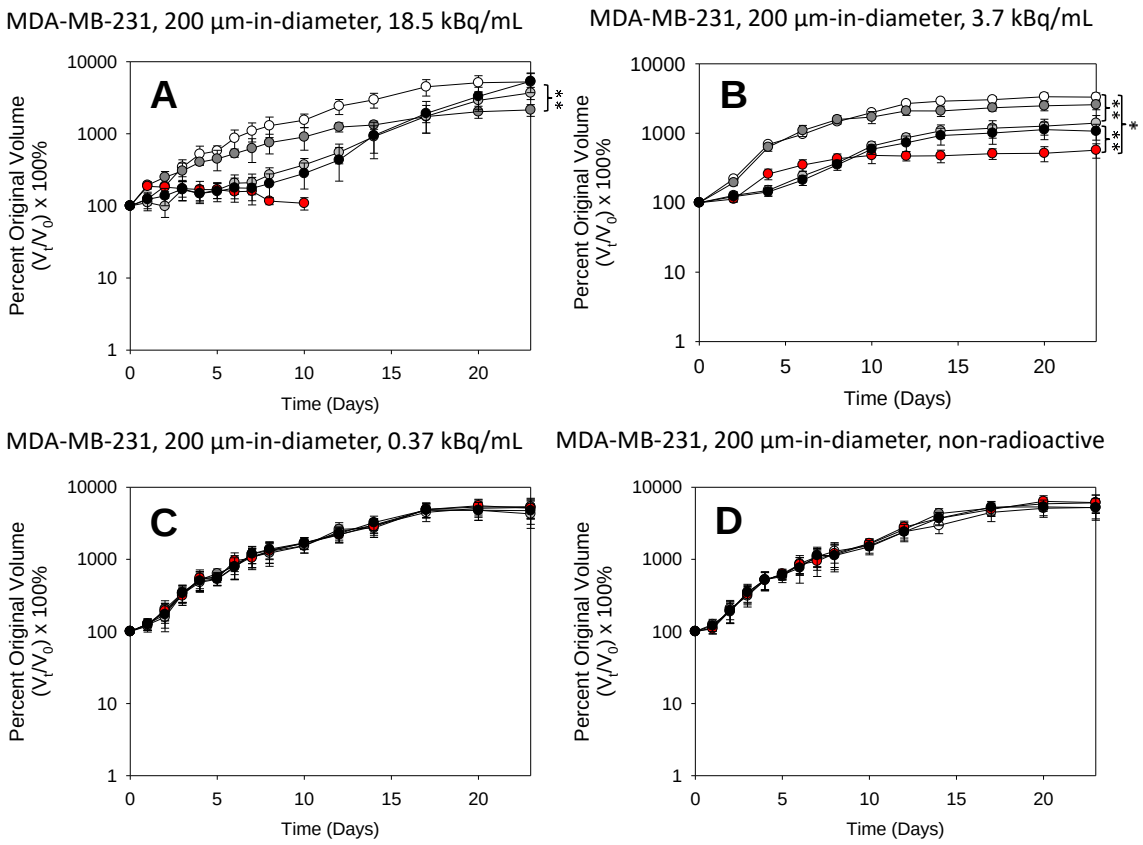


**Figure 4.11.** Efficacy of $^{225}$Ac constructs on 200 µm-in-diameter MDA-MB-231 spheroids. Spheroids were treated at (A) 18.5, (B) 3.7, (C) 0.37, or (D), 0 kBq/mL radioactivity in the form of non-pH-responsive liposomes (grey symbols), radiolabeled trastuzumab (black symbols), radiolabeled isotype control antibody (dark grey symbols), or pH-responsive liposomes (red symbols). White symbols denote media-only negative control and are always non-radioactive. Double asterisks denote $P < 0.05$, while single asterisk denotes $P < 0.01$.

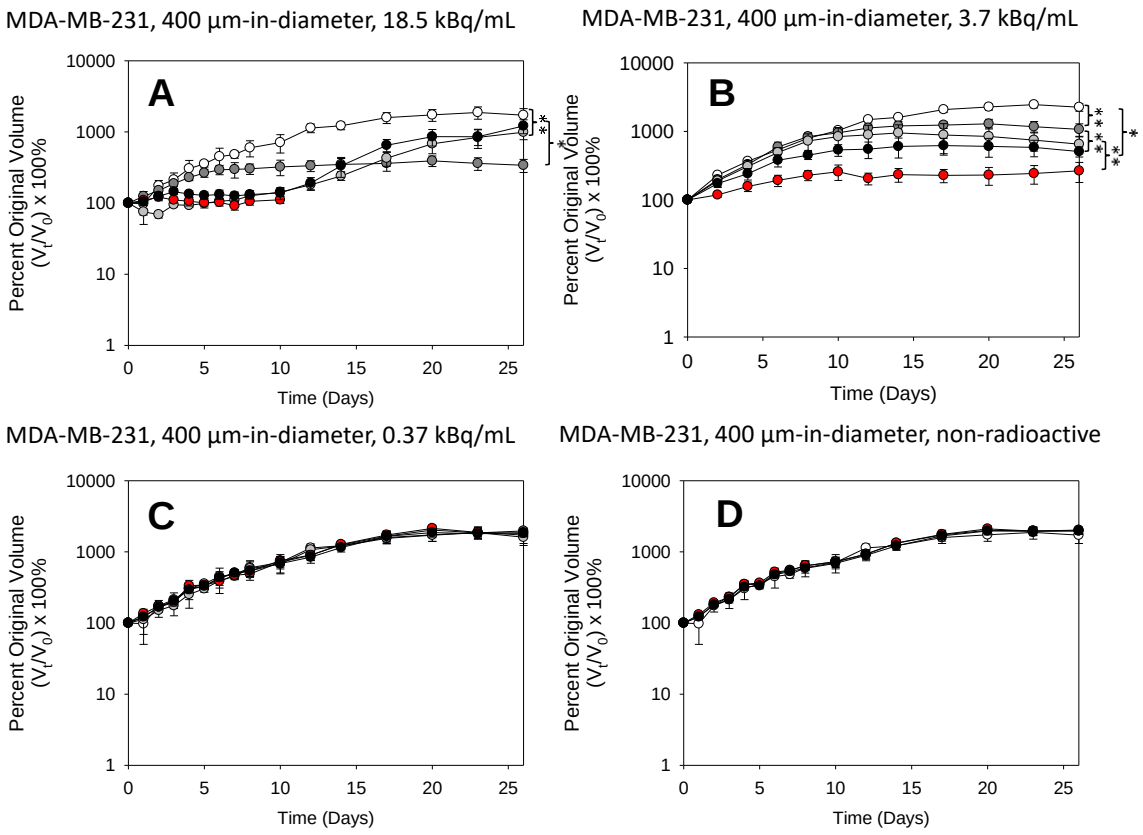


**Figure 4.12.** Efficacy of $^{225}$Ac constructs on 400 µm-in-diameter MDA-MB-231 spheroids. Spheroids were treated at (A) 18.5, (B) 3.7, (C) 0.37, or (D), 0 kBq/mL radioactivity in the form of non-pH-responsive liposomes (grey symbols), radiolabeled trastuzumab (black symbols), radiolabeled isotype control antibody (dark grey symbols), or pH-responsive liposomes (red symbols). White symbols denote media-only negative control and are always non-radioactive. Double asterisks denote $P < 0.05$, while single asterisk denotes $P < 0.01$.

Due to the initiation of MDA-MB-231 spheroids in the presence of Matrigel™, which solidifies into a gel at temperatures higher than 6°C, spheroids without viable cells left behind a Matrigel™ "skeleton," which persisted in the absence of cells. After visual inspection on spheroids suggested a lack of viable cells, MDA-MB-231 spheroid "skeletons" previously treated with $^{225}$Ac-loaded pH-releasing liposomes were plated on cell culture wells to allow outgrowth of viable cells onto the well surface (Figure 4.13).

As expected, plating of MDA-MB-231 Matrigel™ “skeletons” did not result in cell proliferation, suggesting a lack of viable cells.

As a negative control, spheroids of both cell lines and sizes were incubated with nonradioactive constructs. Results showed no effect of nonradioactive antibodies or liposomes on spheroids, with the exception of trastuzumab on BT474, which was likely due to its therapeutic efficacy on HER2-overexpressing cells (Figure 4.9, 4.10).

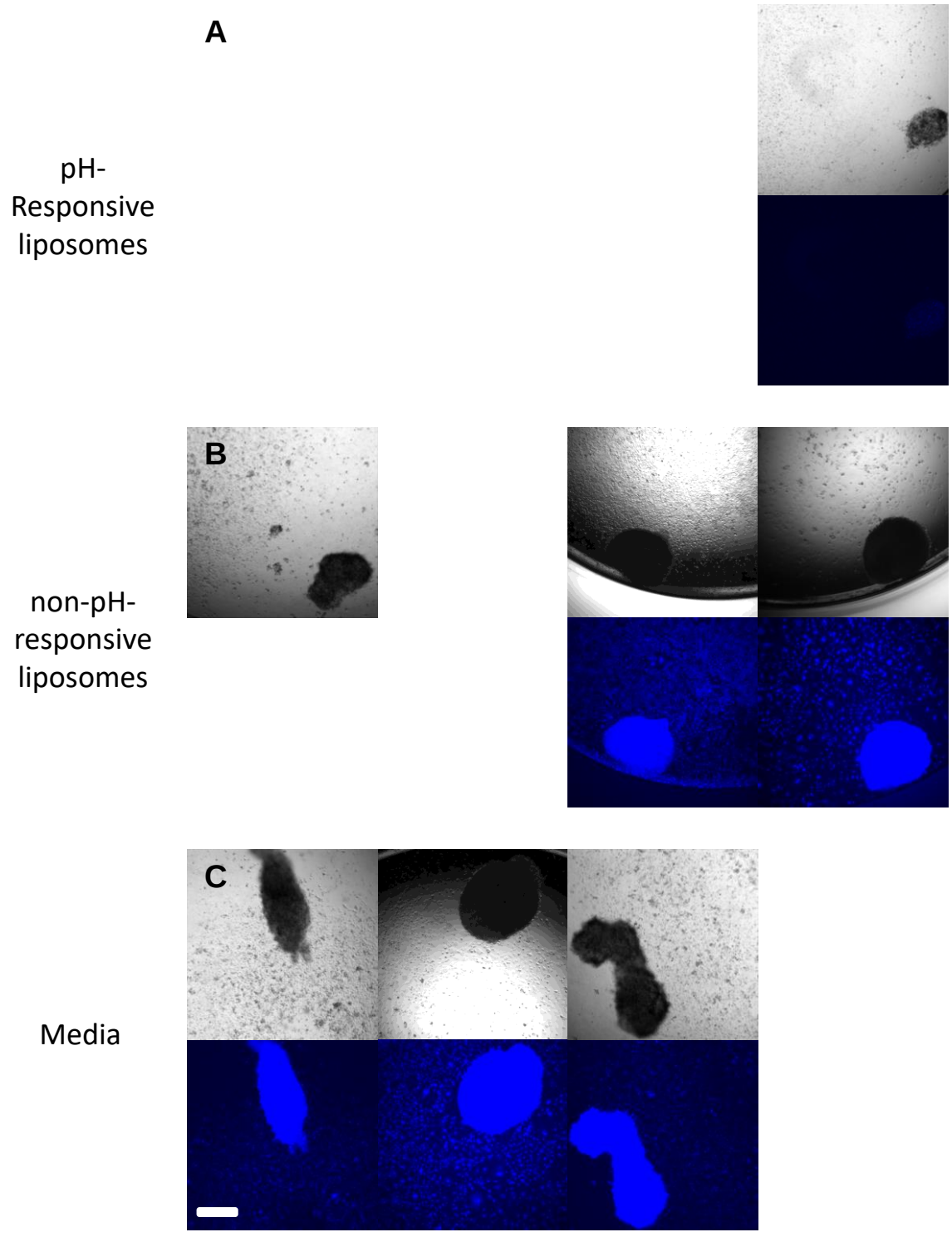


**Figure 4.13.** Bright field and fluorescent (Hoechst 33342 stain under blue channel) images of outgrowth of MDA-MB-231 spheroids following treatment with (A) 18.5 kBq/mL pH-responsive liposomes, (B), 18.5 kBq/mL non-pH-responsive liposomes, and (C) media.

*Alpha Camera and γH2AX imaging*

Alpha camera imaging of $^{225}$Ac distribution throughout spheroid slices gave similar results to that of fluorescent imaging of calcein. Actinium-225 delivered via non-pH-responsive liposomes or antibodies failed to penetrate throughout the entire spheroid volume and accumulate at the periphery, whereas $^{225}$Ac delivered via pH-responsive liposomes demonstrated  a more homogeneous distribution throughout the spheroid volume (Figure 4.14).

Fluorescence staining and imaging of γH2AX intensity across spheroids treated with $^{225}$Ac-trastuzumab or $^{225}$Ac-loaded non-pH releasing liposomes resulted in the highest γH2AX signal at the spheroid periphery, which gradually decreased as a function of radial diameter until there was roughly minimal signal at approximately 120 μm depth into the spheroid (Figure 4.14). In contrast, spheroids treated with $^{225}$Ac-loaded pH-releasing liposomes exhibited a higher signal of γH2AX at the spheroid core, which indicated the presence of dsDNA breaks and corresponded well to intra-spheroid location of $^{225}$Ac as determined by alpha camera.

**Figure 4.14.** Actinium-225 distributions (left) and γH2AX imaging (right) of BT-474 (A) and MDA-MB-231 (B) spheroids. Scale bar is 400 μm.

*In Vivo Studies*

The MTD, defined as the dose at which no mouse suffered death or required euthanasia per IACUC protocol, was determined to be 400 nCi per tumor free animal of approximately 20 gr weight. Tumor bearing mice, once reaching approximately 100 $mm^3$ tumor volume and thus receiving treatment, survived a median of 24 days after therapy when receiving saline, $^{225}$Ac-loaded non-pH-responsive liposomes or radiolabeled trastuzumab, and 36 days when receiving $^{225}$Ac-loaded pH-responsive liposomes (Figure 4.15; $p < 0.05$). Tumor volumes over time showed slower tumor growth within the group treated with pH-responsive liposomes.

**A** **B**

| Group 1 | Group 2 | P-value |
|---|---|---|
| pH-Releasing Liposomes | Non-Releasing Liposomes | 0.009 |
| pH-Releasing Liposomes | Antibody | 0.026 |
| pH-Releasing Liposomes | Saline | 0.023 |
| Non-Releasing Liposomes | Antibody | 0.397 |
| Non-Releasing Liposomes | Saline | 0.5 |
| Antibody | Saline | 0.184 |

**Figure 4.15.** (A) Overall survival and (B) corresponding tumor volume growth of athymic nude mice bearing orthotopic xenograft tumors in the mammary fat pad following therapy with various $^{225}$Ac constructs or saline. Error bars correspond to standard error of the mean.

## 4.4 Discussion

In this study, we have described the use of environmentally-responsive liposomes that release highly diffusive constructs of $^{225}$Ac to improve the drug distribution throughout spheroids, an *in vitro* analogue of the avascular portion of solid tumors. Nanoparticles such as 100 nm liposomes are known to extravasate through leaky tumor vasculature into solid tumor space via the enhanced permeability and retention (EPR) effect. However, extravasated nanoparticles do not penetrate very far into the interstitial space, resulting in heterogeneous drug distribution. The use of antibodies on solid tumor therapy is limited by the binding site barrier effect [67] in which target receptor binding, internalization, and recycling act as a sink that prevents antibodies from deep penetration. Multiple drug delivery strategies have been developed to overcome this limitation, such

as the use of thermally-responsive liposomes that can be triggered to de-stabilize and release drug contents via mild hyperthermia [68]. Our approach is advantageous in that it does not require external stimuli.

Although our liposomal construct exhibits poor tumor penetration similar to other nanoparticle-based systems, the limited penetration into spheroids is sufficient to reach the slightly acidic pH required to trigger drug release. The effectiveness of our system is demonstrated through the enhanced therapeutic efficacy on larger spheroids between pH-triggered and conventional liposomes as well as the presence of alpha-particle radioactivity and corresponding γH2AX signal in the core of large spheroids.

An interesting result we observed was that $^{225}$Ac-trastuzumab was more effective than $^{225}$Ac-loadedpH-triggered liposomes on 200 μm BT474 spheroids, while the reverse was true on 400 μm BT474 spheroids. Given the penetration depth of trastuzumab on BT474 spheroids after a treatment time of 6 hours (~30 and ~40 μm for 200 and 400 μm diameter, respectively) and the maximum tissue penetration range of alpha-particles within the decay chain of $^{225}$Ac (80 μm from $^{213}$Bi decay), we believe that the entire volume of 200 μm spheroids can be irradiated with $^{225}$Ac-trastuzumab treatment. On the other hand, an inner core of ~160 μm diameter remains unexposed to alpha-particle irradiation on 400 μm spheroids. This phenomenon on 400 μm spheroids can be visualized on our alpha camera results. A microdosimetric model is in development by our collaborators that aims to quantitatively support our claims.

# CHAPTER 5: DISSERTATION SUMMARY

## 5.1 Key Findings

The key finding of this dissertation is that liposome-mediated delivery of alpha particle radionuclides for the therapy of solid tumors may be a viable therapy option. More specifically, we have demonstrated that: (1) liposomal alpha particle emitters are potential therapeutics for tumor vasculature, (2) intracellular trafficking and localization of internalized alpha particle emitters affects the tumor cell killing efficacy, and (3) triggered release of highly diffusive species of $^{225}$Ac within solid tumor interstitium improves killing of large multicellular spheroids *in vitro and controls to a great extent tumor growth in vivo*. These findings are significant for several reasons: (1) targeted alpha therapy is currently dominated by radiolabeled antibodies, which currently possess disadvantages such as low specific activity (one $^{225}$Ac radionuclide per 25 – 2000 unlabeled antibodies, depending on radiolabeling chemistry, compared to three $^{225}$Ac per two liposomes), (2) intracellular localization has not previously been a serious consideration for targeted alpha therapy due to a pathlength that traverses a few cell diameters, but our findings suggest that it can play a significant role in cell kill, and (3) alpha-particle emitters have generally been overlooked as a therapeutic option for bulky solid tumors due to the short emission range, but our findings suggest methods of overcoming these physical limitations to direct the unmatched killing efficacy of alpha particles towards solid tumors.

### 5.2 Limitations and future studies

The entirety of the dissertation work described in Chapters 2 and 3 was performed on *in vitro* analogues of tumor endothelium. Although we have demonstrated the anti-vascular potential of $^{225}$Ac-liposomes as well as the effect of intracellular trafficking on killing efficacy, whether these promising *in vitro* results translate to improved outcomes within *in vivo* animal models remains unknown. As previously described in the dissertation, challenges to a reliable *in vivo* model for prostate specific membrane antigen (PSMA) targeted anti-vascular therapy include the unavailability of tumor endothelial cell cultures [60], and host-origin neovasculature in animal tumors. A previous animal study used canine hemangiosarcoma (cHSA) cells, a malignant cancer cell line composed entirely of PSMA-expressing endothelial cells that forms solid tumors and are targetable by the A10 aptamer, in mice as a preclinical tumor vasculature model [69]. However, it is still important to note that the PSMA expressed by cHSA are not of human origin, and that the physiology of the solid tumor formed by endothelial cells may not be an accurate representation of solid tumors.

Another potential area of improvement in the approach we used in Chapters 2 and 3 may be to increase the density of targeting ligands by clustering them into effective "sticky patches" along the liposome surface. This approach, using pH as a trigger, has been previously described by our lab to specifically bind to triple negative breast cancer cells with low target receptor expression [61]. Briefly, targeting ligands homogenously spread across the liposome surface result in nanoparticles that do not specifically bind to low-expressing cells presenting fewer than 90,000 copies of human epidermal growth factor-2 (HER2) receptor. However, by clustering the ligands together to form a "sticky

patch," those same liposomes are capable of specifically binding to triple negative breast cancer cell lines such as MDA-MB-231 (~85,000 HER2/cell) and delivering a cytotoxic dose of doxorubicin. A similar approach of ligand clustering with PSMA-targeting moieties could be investigated on our *in vitro* model, wherein human umbilical vein endothelial cells (HUVEC) express ~52,000 PSMA/cell.

The work described in Chapter 4 of this dissertation investigates the potential of $^{225}$Ac in the therapy of solid tumors. One major area of improvement we have identified is with respect to the clearance rates of liposomes from our multicellular spheroids. Spheroids that uptake liposomes and then subsequently incubated in fresh media are nearly devoid of liposomes after 4 hours of clearance. By increasing the residence time of liposomes within the tumor following therapy, we can effectively improve the therapeutic dose to the tumor without increasing the amount of administered drug. The group's current studies are focused along this direction.

**5.3 References**

1. Howlader N, N.A., Krapcho M, Neyman N, Aminou R, Waldron W, Altekruse SF, Kosary CL, Ruhl J, Tatalovich Z, Cho H, Mariotto A, Eisner MP, Lewis DR, Chen HS, Feuer EJ, Cronin KA, Edwards BK (eds), *SEER Cancer Statistics Review, 1975-2013.* National Cancer Institute. Bethesda, MD, 2016.
2. *Actinium Pharmaceuticals. Study of Iomab-B Prior to HCT vs. Conventional Care in Older Subjects with Active, Relapsed or Refractory AML (SIERRA).* In: ClinicalTrials.gov [Internet]. Bethesda (MD): National Library of Medicine (US). Available from: https://clinicaltrials.gov/ct2/show/NCT02665065, 2016.

3. Zalutsky, M.R. and M. Pruszynski, *Astatine-211: Production and Availability.* Curr Radiopharm, 2011. **4**(3): p. 177-85.

4. Meredith, R.F., J. Torgue, M.T. Azure, S. Shen, S. Saddekni, E. Banaga, R. Carlise, P. Bunch, D. Yoder, and R. Alvarez, *Pharmacokinetics and Imaging of (212)Pb-TCMC-Trastuzumab After Intraperitoneal Administration in Ovarian Cancer Patients.* Cancer Biother Radiopharm, 2014. **29**(1): p. 12-7.

5. Morgenstern, A., F. Bruchertseifer, and C. Apostolidis, *Bismuth-213 and actinium-225 -- generator performance and evolving therapeutic applications of two generator-derived alpha-emitting radioisotopes.* Curr Radiopharm, 2012. **5**(3): p. 221-7.

6. Sgouros, G., *Alpha-particles for targeted therapy.* Adv Drug Deliv Rev, 2008. **60**(12): p. 1402-6.

7. McDevitt, M.R., G. Sgouros, R.D. Finn, J.L. Humm, J.G. Jurcic, S.M. Larson, and D.A. Scheinberg, *Radioimmunotherapy with alpha-emitting nuclides.* Eur J Nucl Med, 1998. **25**(9): p. 1341-51.

8. Sofou, S., *Radionuclide carriers for targeting of cancer.* Int J Nanomedicine, 2008. **3**(2): p. 181-99.

9. Humm, J.L. and L.M. Chin, *A model of cell inactivation by alpha-particle internal emitters.* Radiat Res, 1993. **134**(2): p. 143-50.

10. Humm, J.L., *A microdosimetric model of astatine-211 labeled antibodies for radioimmunotherapy.* Int J Radiat Oncol Biol Phys, 1987. **13**(11): p. 1767-73.

11. Macklis, R.M., B.M. Kinsey, A.I. Kassis, J.L. Ferrara, R.W. Atcher, J.J. Hines, C.N. Coleman, S.J. Adelstein, and S.J. Burakoff, *Radioimmunotherapy with alpha-particle-emitting immunoconjugates.* Science, 1988. **240**(4855): p. 1024-6.

12. Bhagat, M., S. Halligan, and S. Sofou, *Nanocarriers to solid tumors: considerations on tumor penetration and exposure of tumor cells to therapeutic agents.* Curr Pharm Biotechnol, 2012. **13**(7): p. 1306-16.

13. Thurber, G.M., S.C. Zajic, and K.D. Wittrup, *Theoretic criteria for antibody penetration into solid tumors and micrometastases.* J Nucl Med, 2007. **48**(6): p. 995-9.

14. Zaidi H, S.G., eds, *Therapeutic applications of monte carlo calculations in nuclear medicine.* Bristol:IoP, 2003.

15. *Actinium Pharmaceuticals. Low Dose Cytarabine and Lintuzumab-Ac225 in Older AML Patients.* In: ClinicalTrials.gov [Internet]. Bethesda (MD): National Library of Medicine (US). Available from: https://clinicaltrials.gov/ct2/show/NCT02575963, 2016.

16. Mirzadeh, S., *Generator-produced alpha-emitters.* Applied Radiation and Isotopes, 1998. **49**(4): p. 345-349.

17. McDevitt, M.R., D. Ma, J. Simon, R.K. Frank, and D.A. Scheinberg, *Design and synthesis of 225Ac radioimmunopharmaceuticals.* Appl Radiat Isot, 2002. **57**(6): p. 841-7.

18. Deal, K.A., I.A. Davis, S. Mirzadeh, S.J. Kennel, and M.W. Brechbiel, *Improved in vivo stability of actinium-225 macrocyclic complexes.* J Med Chem, 1999. **42**(15): p. 2988-92.

19. Sofou, S. and G. Sgouros, *Antibody-targeted liposomes in cancer therapy and imaging.* Expert Opin Drug Deliv, 2008. **5**(2): p. 189-204.

20. Miederer, M., D.A. Scheinberg, and M.R. McDevitt, *Realizing the potential of the Actinium-225 radionuclide generator in targeted alpha particle therapy applications.* Adv Drug Deliv Rev, 2008. **60**(12): p. 1371-82.

21. Sun, H. and K.Y. Szeto, *Binding of bismuth to serum proteins: implication for targets of Bi(III) in blood plasma.* J Inorg Biochem, 2003. **94**(1-2): p. 114-20.

22. Miquel, G., T. Nekaa, P.H. Kahn, M. Hemadi, and J.M. El Hage Chahine, *Mechanism of formation of the complex between transferrin and bismuth, and interaction with transferrin receptor 1.* Biochemistry, 2004. **43**(46): p. 14722-31.

23. Miederer, M., M.R. McDevitt, G. Sgouros, K. Kramer, N.K. Cheung, and D.A. Scheinberg, *Pharmacokinetics, dosimetry, and toxicity of the targetable atomic generator, 225Ac-HuM195, in nonhuman primates.* J Nucl Med, 2004. **45**(1): p. 129-37.

24. Jurcic, J.G., F. Ravandi, J.M. Pagel, J.H. Park, B.D. Smith, M.Y. Levy, E.H. Estey, A.E. Perl, H. Kantarjian, D. Earle, D. Cicic, and D.A. Scheinberg, * Phase I Trial of Targeted Alpha-Particle Immunotherapy with Actinium-225 (<sup>225</sup>Ac)-Lintuzumab (Anti-CD33) and Low-Dose Cytarabine (LDAC) in Older Patients with Untreated Acute Myeloid Leukemia (AML) *. Blood, 2015. **126**(23): p. 3794-3794.

25. Sofou, S., B.J. Kappel, J.S. Jaggi, M.R. McDevitt, D.A. Scheinberg, and G. Sgouros, *Enhanced retention of the alpha-particle-emitting daughters of Actinium-225 by liposome carriers.* Bioconjug Chem, 2007. **18**(6): p. 2061-7.

26. Wang, G., R.M. de Kruijff, A. Rol, L. Thijssen, E. Mendes, A. Morgenstern, F. Bruchertseifer, M.C. Stuart, H.T. Wolterbeek, and A.G. Denkova, *Retention studies of recoiling daughter nuclides of 225Ac in polymer vesicles.* Appl Radiat Isot, 2014. **85**: p. 45-53.

27. McLaughlin, M.F., D. Robertson, P.H. Pevsner, J.S. Wall, S. Mirzadeh, and S.J. Kennel, *LnPO4 nanoparticles doped with Ac-225 and sequestered daughters for targeted alpha therapy.* Cancer Biother Radiopharm, 2014. **29**(1): p. 34-41.

28. Woodward, J., S.J. Kennel, A. Stuckey, D. Osborne, J. Wall, A.J. Rondinone, R.F. Standaert, and S. Mirzadeh, *LaPO4 nanoparticles doped with actinium-225 that partially sequester daughter radionuclides.* Bioconjug Chem, 2011. **22**(4): p. 766-76.

29. Sempkowski, M., T. Locke, S. Stras, C. Zhu, and S. Sofou, *Liposome-based approaches for delivery of mainstream chemotherapeutics: preparation methods, liposome designs, therapeutic efficacy.* Crit Rev Oncog, 2014. **19**(3-4): p. 177-221.

30. Alaouie, A.M. and S. Sofou, *Liposomes with Triggered Content Release for Cancer Therapy.* Journal of Biomedical Nanotechnology, 2008. **4**(3): p. 234-244.

31. Zhang, Q., J. Tang, L. Fu, R. Ran, Y. Liu, M. Yuan, and Q. He, *A pH-responsive α-helical cell penetrating peptide-mediated liposomal delivery system.* Biomaterials, 2013. **34**(32): p. 7980-7993.

32. Bandekar, A., C. Zhu, A. Gomez, M.Z. Menzenski, M. Sempkowski, and S. Sofou, *Masking and triggered unmasking of targeting ligands on liposomal*

*chemotherapy selectively suppress tumor growth in vivo.* Mol Pharm, 2013. **10**(1): p. 152-60.

33. Li, L., T.L. ten Hagen, M. Hossann, R. Suss, G.C. van Rhoon, A.M. Eggermont, D. Haemmerich, and G.A. Koning, *Mild hyperthermia triggered doxorubicin release from optimized stealth thermosensitive liposomes improves intratumoral drug delivery and efficacy.* J Control Release, 2013. **168**(2): p. 142-50.
34. Bandekar, A., S. Karve, M.Y. Chang, Q. Mu, J. Rotolo, and S. Sofou, *Antitumor efficacy following the intracellular and interstitial release of liposomal doxorubicin.* Biomaterials, 2012. **33**(17): p. 4345-52.
35. Li, L., T.L. ten Hagen, D. Schipper, T.M. Wijnberg, G.C. van Rhoon, A.M. Eggermont, L.H. Lindner, and G.A. Koning, *Triggered content release from optimized stealth thermosensitive liposomes using mild hyperthermia.* J Control Release, 2010. **143**(2): p. 274-9.
36. Chang, M.Y., J. Seideman, and S. Sofou, *Enhanced loading efficiency and retention of 225Ac in rigid liposomes for potential targeted therapy of micrometastases.* Bioconjug Chem, 2008. **19**(6): p. 1274-82.
37. Maguire, W.F., M.R. McDevitt, P.M. Smith-Jones, and D.A. Scheinberg, *Efficient 1-step radiolabeling of monoclonal antibodies to high specific activity with 225Ac for alpha-particle radioimmunotherapy of cancer.* J Nucl Med, 2014. **55**(9): p. 1492-8.
38. Pasternack, J.B., J.D. Domogauer, A. Khullar, J.M. Akudugu, and R.W. Howell, *The advantage of antibody cocktails for targeted alpha therapy depends on specific activity.* J Nucl Med, 2014. **55**(12): p. 2012-9.

39. Liu, T., M. Jabbes, J.R. Nedrow-Byers, L.Y. Wu, J.N. Bryan, and C.E. Berkman, *Detection of prostate-specific membrane antigen on HUVECs in response to breast tumor-conditioned medium.* Int J Oncol, 2011. **38**(5): p. 1349-55.

40. Wu, L.-J., G. Randers-Pehrson, A. Xu, C.A. Waldren, C.R. Geard, Z. Yu, and T.K. Hei, *Targeted cytoplasmic irradiation with alpha particles induces mutations in mammalian cells.* Proceedings of the National Academy of Sciences of the United States of America, 1999. **96**(9): p. 4959-4964.

41. Hei, T.K., L.J. Wu, S.X. Liu, D. Vannais, C.A. Waldren, and G. Randers-Pehrson, *Mutagenic effects of a single and an exact number of alpha particles in mammalian cells.* Proc Natl Acad Sci U S A, 1997. **94**(8): p. 3765-70.

42. Karve, S., G. Bajagur Kempegowda, and S. Sofou, *Heterogeneous domains and membrane permeability in phosphatidylcholine-phosphatidic acid rigid vesicles as a function of pH and lipid chain mismatch.* Langmuir, 2008. **24**(11): p. 5679-88.

43. Karve, S., A. Alaouie, Y. Zhou, J. Rotolo, and S. Sofou, *The use of pH-triggered leaky heterogeneities on rigid lipid bilayers to improve intracellular trafficking and therapeutic potential of targeted liposomal immunochemotherapy.* Biomaterials, 2009. **30**(30): p. 6055-64.

44. Folkman, J., *Tumor angiogenesis: therapeutic implications.* N Engl J Med, 1971. **285**(21): p. 1182-6.

45. Folkman, J., *What is the evidence that tumors are angiogenesis dependent?* J Natl Cancer Inst, 1990. **82**(1): p. 4-6.

46. Brooks, P.C., R.A. Clark, and D.A. Cheresh, *Requirement of vascular integrin alpha v beta 3 for angiogenesis.* Science, 1994. **264**(5158): p. 569-71.

47. Burrows, F.J. and P.E. Thorpe, *Eradication of large solid tumors in mice with an immunotoxin directed against tumor vasculature.* Proc Natl Acad Sci U S A, 1993. **90**(19): p. 8996-9000.

48. Liu, H., P. Moy, S. Kim, Y. Xia, A. Rajasekaran, V. Navarro, B. Knudsen, and N.H. Bander, *Monoclonal antibodies to the extracellular domain of prostate-specific membrane antigen also react with tumor vascular endothelium.* Cancer Res, 1997. **57**(17): p. 3629-34.

49. Liu, H., A.K. Rajasekaran, P. Moy, Y. Xia, S. Kim, V. Navarro, R. Rahmati, and N.H. Bander, *Constitutive and antibody-induced internalization of prostate-specific membrane antigen.* Cancer Res, 1998. **58**(18): p. 4055-60.

50. Lupold, S.E., B.J. Hicke, Y. Lin, and D.S. Coffey, *Identification and characterization of nuclease-stabilized RNA molecules that bind human prostate cancer cells via the prostate-specific membrane antigen.* Cancer Res, 2002. **62**(14): p. 4029-33.

51. Banerjee, S.R., M. Pullambhatla, Y. Byun, S. Nimmagadda, C.A. Foss, G. Green, J.J. Fox, S.E. Lupold, R.C. Mease, and M.G. Pomper, *Sequential SPECT and optical imaging of experimental models of prostate cancer with a dual modality inhibitor of the prostate-specific membrane antigen.* Angew Chem Int Ed Engl, 2011. **50**(39): p. 9167-70.

52. Bandekar, A., C. Zhu, R. Jindal, F. Bruchertseifer, A. Morgenstern, and S. Sofou, *Anti-prostate-specific membrane antigen liposomes loaded with 225Ac for*

*potential targeted antivascular alpha-particle therapy of cancer.* J Nucl Med, 2014. **55**(1): p. 107-14.

53. Farokhzad, O.C., S. Jon, A. Khademhosseini, T.-N.T. Tran, D.A. LaVan, and R. Langer, *Nanoparticle-Aptamer Bioconjugates.* A New Approach for Targeting Prostate Cancer Cells, 2004. **64**(21): p. 7668-7672.

54. Allen, B.J., C. Raja, S. Rizvi, E.Y. Song, and P. Graham, *Tumour anti-vascular alpha therapy: a mechanism for the regression of solid tumours in metastatic cancer.* Phys Med Biol, 2007. **52**(13): p. L15-9.

55. Behling, K., W.F. Maguire, J.C. Puebla, S.R. Sprinkle, A. Ruggiero, J. O'Donoghue, P.H. Gutin, D.A. Scheinberg, and M.R. McDevitt, *Vascular targeted radioimmunotherapy for the treatment of glioblastoma.* J Nucl Med, 2016.

56. Behling, K., V. DiGialleonardo, W.F. Maguire, L.E. Heeb, I.F. Hassan, D.R. Veach, K.R. Keshari, P.H. Gutin, D.A. Scheinberg, and M.R. McDevitt, *Remodelling the vascular microenvironment of glioblastoma with alpha-particles.* J Nucl Med, 2016.

57. Ansell, S.M., T.O. Harasym, P.G. Tardi, S.S. Buchkowsky, M.B. Bally, and P.R. Cullis, *Antibody conjugation methods for active targeting of liposomes.* Methods Mol Med, 2000. **25**: p. 51-68.

58. Sofou, S., J.L. Thomas, H.Y. Lin, M.R. McDevitt, D.A. Scheinberg, and G. Sgouros, *Engineered liposomes for potential alpha-particle therapy of metastatic cancer.* J Nucl Med, 2004. **45**(2): p. 253-60.

59. Behr, T.M., M. Behe, M. Lohr, G. Sgouros, C. Angerstein, E. Wehrmann, K. Nebendahl, and W. Becker, *Therapeutic advantages of Auger electron- over beta-emitting radiometals or radioiodine when conjugated to internalizing antibodies.* Eur J Nucl Med, 2000. **27**(7): p. 753-65.

60. Dudley, A.C., *Tumor Endothelial Cells.* Cold Spring Harb Perspect Med, 2012. **2**(3).

61. Sempkowski, M., C. Zhu, M.Z. Menzenski, I.G. Kevrekidis, F. Bruchertseifer, A. Morgenstern, and S. Sofou, *Sticky Patches on Lipid Nanoparticles Enable the Selective Targeting and Killing of Untargetable Cancer Cells.* Langmuir, 2016. **32**(33): p. 8329-38.

62. Jain, R.K. and T. Stylianopoulos, *Delivering nanomedicine to solid tumors.* Nat Rev Clin Oncol, 2010. **7**(11): p. 653-64.

63. Sofou, S., *Surface-active liposomes for targeted cancer therapy.* Nanomedicine (Lond), 2007. **2**(5): p. 711-24.

64. Eary JF, B.W., eds., *Nuclear medicine therapy.* New York: Informa Healthcare Inc, 2007.

65. Back, T. and L. Jacobsson, *The alpha-camera: a quantitative digital autoradiography technique using a charge-coupled device for ex vivo high-resolution bioimaging of alpha-particles.* J Nucl Med, 2010. **51**(10): p. 1616-23.

66. Chouin, N., S. Lindegren, S.H. Frost, H. Jensen, P. Albertsson, R. Hultborn, S. Palm, L. Jacobsson, and T. Back, *Ex vivo activity quantification in micrometastases at the cellular scale using the alpha-camera technique.* J Nucl Med, 2013. **54**(8): p. 1347-53.

67. Graff, C.P. and K.D. Wittrup, *Theoretical analysis of antibody targeting of tumor spheroids: importance of dosage for penetration, and affinity for retention.* Cancer Res, 2003. **63**(6): p. 1288-96.

68. Kono, K., T. Ozawa, T. Yoshida, F. Ozaki, Y. Ishizaka, K. Maruyama, C. Kojima, A. Harada, and S. Aoshima, *Highly temperature-sensitive liposomes based on a thermosensitive block copolymer for tumor-specific chemotherapy.* Biomaterials, 2010. **31**(27): p. 7096-7105.

69. Tang, L., R. Tong, V.J. Coyle, Q. Yin, H. Pondenis, L.B. Borst, J. Cheng, and T.M. Fan, *Targeting tumor vasculature with aptamer-functionalized doxorubicin-polylactide nanoconjugates for enhanced cancer therapy.* ACS Nano, 2015. **9**(5): p. 5072-81.